Hindawi Publishing Corporation
Shock and Vibration
Volume 2016, Article ID 2150493, 20 pages
http://dx.doi.org/10.1155/2016/2150493

Research Article

Observer Based Optimal Vibration Control of a Full Aircraft System Having Active Landing Gears and Biodynamic Pilot Model

Hakan Yazici[1] and Mert Sever[2]

[1]*Department of Mechanical Engineering, Yildiz Technical University, Istanbul, Turkey*
[2]*Department of Mechatronics Engineering, Yildiz Technical University, Istanbul, Turkey*

Correspondence should be addressed to Hakan Yazici; hyazici@yildiz.edu.tr

Received 28 March 2016; Revised 9 August 2016; Accepted 7 September 2016

Academic Editor: Mickaël Lallart

This paper deals with the design of an observed based optimal state feedback controller having pole location constraints for an active vibration mitigation problem of an aircraft system. An eleven-degree-of-freedom detailed full aircraft mathematical model having active landing gears and a seated pilot body is developed to control and analyze aircraft vibrations caused by runway excitation, when the aircraft is taxiing. Ground induced vibration can contribute to the reduction of pilot's capability to control the aircraft and cause the safety problem before take-off and after landing. Since the state variables of the pilot body are not available for measurement in practice, an observed based optimal controller is designed via Linear Matrix Inequalities (LMIs) approach. In addition, classical LQR controller is designed to investigate effectiveness of the proposed controller. The system is then simulated against the bump and random runway excitation. The simulation results demonstrate that the proposed controller provides significant improvements in reducing vibration amplitudes of aircraft fuselage and pilot's head and maintains the safety requirements in terms of suspension stroke and tire deflection.

1. Introduction

The landing of an aircraft is the most critical operation, since it directly affects the safety, comfort, taxiing performance, and aircraft fatigue life [1]. During landing, ground induced vibrations cause the safety and comfort problem, hence need to mitigate quickly. It is well known that most of the nonfatal accidents occur during the landing [2]. The landing gear system is the intermediate element between the aircraft fuselage and the runway [3]. Therefore, a successfully designed landing gear system should be able to provide the aircraft stability and maneuverability after the landing impact [4].

Dynamic and impact loads in aircrafts resulting from landing and uneven runway surfaces are recognized as a significant factor in causing fatigue damage [5]. Additionally, runway irregularities can contribute to reduction of pilot's capability and the accidents may occur because of this problem [1, 6]. Therefore, landing gear systems have to attenuate the ground induced vibrations to improve the passenger-crew safety and comfort.

Design of landing gear systems has been studied for a long time [7–9]. For all aircraft, landing gears are equipped with passive damping devices that suppress the ground induced vibrations [10]. Well-designed passive landing gears can be able to provide the required safety and comfort and absorb the energy during the touchdown [11]. However, the vibration damping performance of the passive landing gear system is not ensured since the passive damper devices cannot be tuned for every single runway's characteristics [12]. Therefore, semiactive and active landing gears systems are currently being studied and experimented to overcome this adaptability problem [13, 14].

In literature, many linear and nonlinear control methods have been proposed for active and semiactive landing gear systems [15, 16]. Ghiringhelli and Gualdi have designed a hybrid semiactive controller that combines a nonlinear PID term to mitigate the ground induced vibrations [17].

Gharapurkar et al. have designed a semiactive magnetorheological landing gear system by the use of Linear Quadratic Regulator (LQR) and H_∞ control methods for a three-degree-of-freedom aircraft model considering the bounce, the pitch, and the roll motions [18]. Sateesh and Maiti have developed a torsional MR damper to enhance the stability of the nose landing gear system due to the ground induced lateral excitation [19].

Among the passive, semiactive, and active landing gears, active landing gears can provide the best comfort and safety performance. Therefore, active landing gears have received much more attention in the last decades. Ross and Edson have designed an active landing gear system to mitigate the landing loads and ground induced vibrations under various runway irregularities in their brief study [20]. Freymann has applied an experimental and analytical study to show the efficiency of active landing gears in reducing landing loads and ground induced vibrations under different runway excitation [21]. A full aircraft model having active landing gears has been considered by Sivakumar and Haran, and PID controllers have been designed to attenuate the ground induced vibrations for passenger comfort and safety while the aircraft is taxiing [22].

All the papers discussed above add some significant contribution to the literature. However, the pilot body vibration analysis in terms of safety and comfort performance requirements has not been considered using detailed full aircraft mathematical model having an integrated biodynamic pilot model so far which is the main motivation factor of this study.

In this paper, landing gear control strategy for a detailed full aircraft with biodynamic pilot model is proposed to improve vibration suppression performance on pilot ride comfort, ride safety, and fuselage acceleration when the aircraft is subjected to runway disturbance during the taxiing. An integrated pilot's seat and detailed full aircraft model that includes Abbas et al.'s [23] four-degree-of-freedom biodynamic seated pilot model is presented. This detailed mathematical model provides a platform to analyze ride comfort performance in terms of pilot's head acceleration responses during taxiing under different type runway excitation. Based on the detailed aircraft mathematical model, an optimal controller is designed to attenuate the fuselage and pilot's head vibrations. Because the state variables of biodynamic pilot body model are not available for measurement in practice, an observer based state feedback optimal controller having pole location constraints is developed using LMIs approach. Additionally, classical LQR controller is designed to demonstrate the effectiveness of the proposed observer based controller. Finally, numerical simulation studies are conducted to evaluate the performance of the designed controller under bump and random type runway excitation.

Rest of the paper is organized as follows: Section 2 describes the dynamic model of a full aircraft system having active landing gears and biodynamic pilot model. The design of an observer based state feedback optimal controller having pole location constraints is presented in Section 3. Simulation results with discussions are given in Section 4. Finally, Section 5 concludes the paper.

Notation. A fairly standard notation is used throughout the paper. $\mathfrak{R}$ stands for the set of real numbers, and $\mathfrak{R}^{n\times n}$ is the set of $n \times n$ dimensional real matrices. "trace" stands for the standard trace operator. The identity and null matrices are denoted by I and 0, respectively. $X > 0$ $(\geq, < 0)$ denotes that X is a positive-definite (positive semidefinite, negative definite) matrix. The notation "$\otimes$" denotes the Kronecker product. Finally, diag$\{M_1, \ldots, M_n\}$ stands for a diagonal matrix with elements $M_1, \ldots, M_n$ appearing on its diagonal.

2. Mathematical Modelling of a Full Aircraft System Having Active Landing Gears and Biodynamic Pilot Model

In this study, an eleven-degree-of-freedom detailed full aircraft model is shown in Figure 1, including active landing gears and a pilot seat suspension system, and an integrated four-degree-of-freedom biodynamic pilot body model is provided. The mathematical model consists of full vehicle dynamics and vertical vibrations of seated pilot body. In this model, aircraft dynamics include vertical motions of fuselage and tires, angular motions of fuselage as known as roll, and pitch.

In Figure 1, m_f is the fuselage body mass which is connected to the three masses of the front, rear left, and rear right landing gears. $m_{\mathrm{t}1}$, $m_{\mathrm{t}2}$, and $m_{\mathrm{t}3}$ are the front, rear left, and rear right landing gear masses, respectively. m_s is the pilot's seat mass, and the pilot body is composed of four-mass segment, that is, head and neck m_h, upper torso m_u, lower torso m_l, and thigh and pelvis m_p. The arms and legs are combined with the upper torso and thigh, respectively [23]. $z_{\mathrm{t}1}(t)$, $z_{\mathrm{t}2}(t)$, and $z_{\mathrm{t}3}(t)$ are the vertical displacements of front, rear left, and rear right tires. $z_\mathrm{f}(t)$ is bounce motion of the fuselage and $\phi(t)$ and $\theta(t)$ are the roll and pitch angular positions which are defined with respect to the body fixed coordinate frame. $z_\mathrm{s}(t)$ is the vertical displacement of pilot's seat. $z_\mathrm{p}(t)$, $z_\mathrm{l}(t)$, $z_\mathrm{u}(t)$, and $z_\mathrm{h}(t)$ are defined as vertical displacements of thigh and pelvis, lower torso, upper torso, and head, respectively. $z_{\mathrm{r}1}(t)$, $z_{\mathrm{r}2}(t)$, and $z_{\mathrm{r}3}(t)$ are the runway displacement inputs. $c_{\mathrm{s}1}, k_{\mathrm{s}1}$, $c_{\mathrm{s}2}, k_{\mathrm{s}2}$, and $c_{\mathrm{s}3}, k_{\mathrm{s}3}$ are the damping and stiffness of the front landing gear system, rear left landing gear system, and rear right landing gear system, respectively. $c_{\mathrm{t}1}, k_{\mathrm{t}1}$, $c_{\mathrm{t}2}, k_{\mathrm{t}2}$, and $c_{\mathrm{t}3}, k_{\mathrm{t}3}$ stand for the damping and stiffness of the front tires, rear left tires, and rear right tires, respectively. Seat suspension stiffness and damping elements are $k_{\mathrm{fs}}, c_{\mathrm{fs}}$. Stiffness and damping elements between seat and pelvis are $k_{\mathrm{sp}}, c_{\mathrm{sp}}$, pelvis and lower torso are $k_{\mathrm{pl}}, c_{\mathrm{pl}}$, pelvis and upper torso are $k_{\mathrm{pu}}, c_{\mathrm{pu}}$, lower torso and upper torso are $k_{\mathrm{lu}}, c_{\mathrm{lu}}$, and upper torso and head are $k_{\mathrm{uh}}, c_{\mathrm{uh}}$, respectively. $F_1(t)$, $F_2(t)$, and $F_3(t)$ represent the active control forces that are applied to the front landing gear, rear left landing gear, and rear right landing gear of modelled aircraft, respectively. ℓ_f and ℓ_r denote the distance from Center of Gravity (CG) to the front and rear landing gear along x_s axis. ℓ_{sl} and ℓ_{sr} denote the distances between CG and rear left landing gear and rear right landing gear y_f direction. Finally, ℓ_{sf} and ℓ_{ss} denote the distances between CG and seat along x_f and y_f directions.

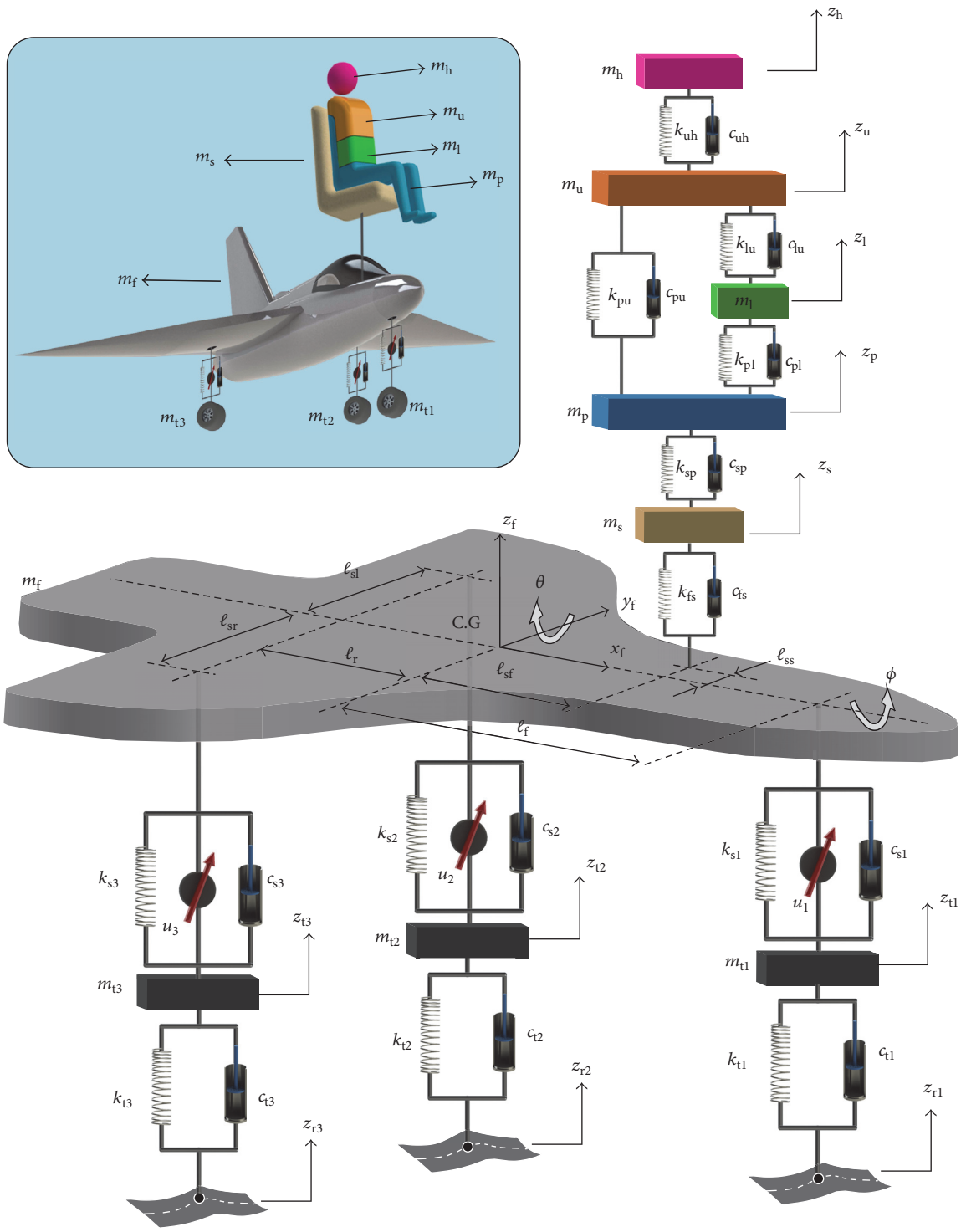

FIGURE 1: Full aircraft vibration model having active landing gears and biodynamic pilot body subject to runway excitation.

2.1. Equilibrium Equations of Motion. The dynamic equilibrium equations of motion for the full aircraft having active landing gear systems, an integrated pilot's seat and biodynamic pilot model, are derived by Lagrange method. The general Lagrange equation can be written as

$$\frac{\mathrm{d}}{\mathrm{d}t}\left(\frac{\partial E_{\mathrm{K}}}{\partial \dot{q}_i}\right) - \frac{\partial E_{\mathrm{K}}}{\partial q_i} + \frac{\partial E_{\mathrm{P}}}{\partial q_i} + \frac{\partial E_{\mathrm{D}}}{\partial \dot{q}_i} = Q_i, \tag{1}$$

where E_{K}, E_{P}, and E_{D} are the kinetic energy, potential energy, and dissipative energy of the system, respectively. q_i

is the generalized coordinates and Q_i is the external forces of the system. The generalized coordinates and forces for the modeled full aircraft system can be written as

$$q(t) = \left[z_{t1}(t)\ \ z_{t2}(t)\ \ z_{t3}(t)\ \ \phi(t)\ \ \theta(t)\ \ z_f(t)\ \ z_s(t)\ \ z_p(t)\ \ z_l(t)\ \ z_u(t)\ \ z_h(t)\right]^T, \tag{2}$$

$$\begin{aligned} &Q(t) \\ &= \left[-F_1(t)\ \ -F_2(t)\ \ -F_3(t)\ \ \ell_{sl}F_2(t) - \ell_{sr}F_3(t)\ \ \ell_r\left(F_2(t) + F_3(t)\right) - \ell_f F_1(t)\ \ F_1(t) + F_2(t) + F_3(t)\ \ 0\ \ 0\ \ 0\ \ 0\ \ 0\right]^T. \end{aligned} \tag{3}$$

In order to obtain the kinetic energy, potential energy, and dissipative energy of the full aircraft system, deflections of each stiffness and damping element are defined as follows:

$$d_{t1}(t) = z_{t1}(t) - z_{r1}(t), \tag{4}$$

$$d_{t2}(t) = z_{t2}(t) - z_{r2}(t), \tag{5}$$

$$d_{t3}(t) = z_{t3}(t) - z_{r3}(t), \tag{6}$$

$$\begin{aligned} d_{s1}(t) &= z_f(t) - \ell_f \sin\theta(t) - z_{t1}(t) \\ &\cong z_f(t) - \ell_f\theta(t) - z_{t1}(t), \end{aligned} \tag{7}$$

$$\begin{aligned} d_{s2}(t) &= z_f(t) + \ell_r \sin\theta(t) + \ell_{sl}\sin\phi(t) - z_{t2}(t) \\ &\cong z_f(t) + \ell_r\theta(t) + \ell_{sl}\phi(t) - z_{t2}(t), \end{aligned} \tag{8}$$

$$\begin{aligned} d_{s3}(t) &= z_f(t) + \ell_r \sin\theta(t) - \ell_{sr}\sin\phi(t) - z_{t3}(t) \\ &\cong z_f(t) + \ell_r\theta(t) - \ell_{sr}\phi(t) - z_{t3}(t), \end{aligned} \tag{9}$$

$$d_{fs}(t) = z_s(t) - z_f(t) + \ell_{sf}\theta(t) - \ell_{ss}\phi(t), \tag{10}$$

$$d_{sp}(t) = z_p(t) - z_s(t), \tag{11}$$

$$d_{pl}(t) = z_l(t) - z_p(t), \tag{12}$$

$$d_{pu}(t) = z_u(t) - z_p(t), \tag{13}$$

$$d_{lu}(t) = z_u(t) - z_l(t), \tag{14}$$

$$d_{uh}(t) = z_h(t) - z_u(t). \tag{15}$$

By the use of (4)–(15), kinetic, potential, and dissipative energy functions of the full aircraft system can be written as

$$\begin{aligned} E_K &= \frac{1}{2}m_{t1}\dot{z}_{t1}^2(t) + \frac{1}{2}m_{t2}\dot{z}_{t2}^2(t) + \frac{1}{2}m_{t3}\dot{z}_{t3}^2(t) \\ &\quad + \frac{1}{2}I_x\dot{\phi}^2(t) + \frac{1}{2}I_y\dot{\theta}^2(t) + \frac{1}{2}m_f\dot{z}_f^2(t) \\ &\quad + \frac{1}{2}m_s\dot{z}_s^2(t) + \frac{1}{2}m_p\dot{z}_p^2(t) + \frac{1}{2}m_l\dot{z}_l^2(t) \\ &\quad + \frac{1}{2}m_u\dot{z}_u^2(t) + \frac{1}{2}m_h\dot{z}_h^2(t), \\ E_P &= \frac{1}{2}k_{t1}d_{t1}^2(t) + \frac{1}{2}k_{t2}d_{t2}^2(t) + \frac{1}{2}k_{t3}d_{t3}^2(t) \\ &\quad + \frac{1}{2}k_{s1}d_{s1}^2(t) + \frac{1}{2}k_{s2}d_{s2}^2(t) + \frac{1}{2}k_{s3}d_{s3}^2(t) \\ &\quad + \frac{1}{2}k_{fs}d_{fs}^2(t) + \frac{1}{2}k_{sp}d_{sp}^2(t) + \frac{1}{2}k_{pl}d_{pl}^2(t) \\ &\quad + \frac{1}{2}k_{pu}d_{pu}^2(t) + \frac{1}{2}k_{lu}d_{lu}^2(t) + \frac{1}{2}k_{uh}d_{uh}^2(t), \\ E_D &= \frac{1}{2}c_{t1}\dot{d}_{t1}^2(t) + \frac{1}{2}c_{t2}\dot{d}_{t2}^2(t) + \frac{1}{2}c_{t3}\dot{d}_{t3}^2(t) \\ &\quad + \frac{1}{2}c_{s1}\dot{d}_{s1}^2(t) + \frac{1}{2}c_{s2}\dot{d}_{s2}^2(t) + \frac{1}{2}c_{s3}\dot{d}_{s3}^2(t) \\ &\quad + \frac{1}{2}c_{fs}\dot{d}_{fs}^2(t) + \frac{1}{2}c_{sp}\dot{d}_{sp}^2(t) + \frac{1}{2}c_{pl}\dot{d}_{pl}^2(t) \\ &\quad + \frac{1}{2}c_{pu}\dot{d}_{pu}^2(t) + \frac{1}{2}c_{lu}\dot{d}_{lu}^2(t) + \frac{1}{2}c_{uh}\dot{d}_{uh}^2(t). \end{aligned} \tag{16}$$

The energy functions (16) can be used to construct the equilibrium equations of motion by substituting them into Lagrange equation (3) for each generalized coordinate. The governing equilibrium equations of motion for the full aircraft having active landing gear systems, an integrated pilot's seat and biodynamic pilot model, are obtained using Lagrange method as follows:

For front landing gear motion,

$$\begin{aligned} m_{t1}\ddot{z}_{t1}(t) &= -k_{t1}\left[z_{t1}(t) - z_{r1}(t)\right] \\ &\quad - k_{s1}\left[z_{t1}(t) - z_f(t) + \ell_f\theta(t)\right] \\ &\quad - c_{t1}\left[\dot{z}_{t1}(t) - \dot{z}_{r1}(t)\right] \\ &\quad - c_{s1}\left[\dot{z}_{t1}(t) - \dot{z}_f(t) + \ell_f\dot{\theta}(t)\right] - F_1(t). \end{aligned} \tag{17}$$

For rear left landing gear motion,

$$\begin{aligned} m_{t2}\ddot{z}_{t2}(t) &= -k_{t2}\left[z_{t2}(t) - z_{r2}(t)\right] \\ &\quad - k_{s2}\left[z_{t2}(t) - z_f(t) - \ell_r\theta(t) - \ell_{sl}\phi(t)\right] \\ &\quad - c_{t2}\left[\dot{z}_{t2}(t) - \dot{z}_{r2}(t)\right] \\ &\quad - c_{s2}\left[\dot{z}_{t2}(t) - \dot{z}_f(t) - \ell_r\dot{\theta}(t) - \ell_{sl}\dot{\phi}(t)\right] \\ &\quad - F_2(t). \end{aligned} \tag{18}$$

For rear right landing gear motion,

$$\begin{aligned} m_{t3}\ddot{z}_{t3}(t) = &-k_{t3}\left[z_{t3}(t) - z_{r3}(t)\right] \\ &- k_{s3}\left[z_{t3}(t) - z_f(t) - \ell_r\theta(t) + \ell_{sr}\phi(t)\right] \\ &- c_{t3}\left[\dot{z}_{t3}(t) - \dot{z}_{r3}(t)\right] \\ &- c_{s3}\left[\dot{z}_{t3}(t) - \dot{z}_f(t) - \ell_r\dot{\theta}(t) + \ell_{sr}\dot{\phi}(t)\right] \\ &- F_3(t). \end{aligned} \tag{19}$$

For roll motion of the fuselage,

$$\begin{aligned} I_x\ddot{\phi}(t) = &-\ell_{sl}k_{s2}\left[\ell_{sl}\phi(t) + z_f(t) + \ell_r\theta(t) - z_{t2}(t)\right] \\ &- \ell_{sr}k_{s3}\left[\ell_{sr}\phi(t) - z_f(t) - \ell_r\theta(t) + z_{t3}(t)\right] \\ &- \ell_{ss}k_{fs}\left[\ell_{ss}\phi(t) - z_s(t) + z_f(t) - \ell_{sf}\theta(t)\right] \\ &- \ell_{sl}c_{s2}\left[\ell_{sl}\dot{\phi}(t) + \dot{z}_f(t) + \ell_r\dot{\theta}(t) - \dot{z}_{t2}(t)\right] \\ &- \ell_{sr}c_{s3}\left[\ell_{sr}\dot{\phi}(t) - \dot{z}_f(t) - \ell_r\dot{\theta}(t) + \dot{z}_{t3}(t)\right] \\ &- \ell_{ss}c_{fs}\left[\ell_{ss}\dot{\phi}(t) - \dot{z}_s(t) + \dot{z}_f(t) - \ell_{sf}\dot{\theta}(t)\right] \\ &+ \ell_{sl}F_2(t) - \ell_{sr}F_3(t). \end{aligned} \tag{20}$$

For pitch motion of the fuselage,

$$\begin{aligned} I_y\ddot{\theta}(t) = &-\ell_f k_{s1}\left[\ell_f\theta(t) - z_f(t) + z_{t1}(t)\right] \\ &- \ell_r k_{s2}\left[\ell_r\theta(t) + z_f(t) + \ell_{sl}\phi(t) - z_{t2}(t)\right] \\ &- \ell_r k_{s3}\left[\ell_r\theta(t) + z_f(t) - \ell_{sr}\phi(t) - z_{t3}(t)\right] \\ &- \ell_{sf}k_{fs}\left[\ell_{sf}\theta(t) + z_s(t) - z_f(t) - \ell_{ss}\phi(t)\right] \\ &- \ell_f c_{s1}\left[\ell_f\dot{\theta}(t) - \dot{z}_f(t) + \dot{z}_{t1}(t)\right] \\ &- \ell_r c_{s2}\left[\ell_r\dot{\theta}(t) + \dot{z}_f(t) + \ell_{sl}\dot{\phi}(t) - \dot{z}_{t2}(t)\right] \\ &- \ell_r c_{s3}\left[\ell_r\dot{\theta}(t) + \dot{z}_f(t) - \ell_{sr}\dot{\phi}(t) - \dot{z}_{t3}(t)\right] \\ &- \ell_{sf}c_{fs}\left[\ell_{sf}\dot{\theta}(t) + \dot{z}_s(t) - \dot{z}_f(t) - \ell_{ss}\dot{\phi}(t)\right] \\ &+ \ell_r\left[F_2(t) + F_3(t)\right] - \ell_f F_1(t). \end{aligned} \tag{21}$$

For bounce motion of the fuselage,

$$\begin{aligned} m_f\ddot{z}_f(t) = &-k_{fs}\left[z_f(t) - z_s(t) - \ell_{sf}\theta(t) + \ell_{ss}\phi(t)\right] \\ &- k_{s1}\left[z_f(t) - \ell_f\theta(t) - z_{t1}(t)\right] \\ &- k_{s2}\left[z_f(t) + \ell_r\theta(t) + \ell_{sl}\phi(t) - z_{t2}(t)\right] \\ &- k_{s3}\left[z_f(t) + \ell_r\theta(t) - \ell_{sr}\phi(t) - z_{t3}(t)\right] \\ &- k_{t1}\left[z_f(t) - z_{t1}(t)\right] \\ &- k_{t2}\left[z_f(t) - z_{t2}(t)\right] \\ &- k_{t3}\left[z_f(t) - z_{t3}(t)\right] \\ &- c_{fs}\left[\dot{z}_f(t) - \dot{z}_s(t) - \ell_{sf}\dot{\theta}(t) + \ell_{ss}\dot{\phi}(t)\right] \\ &- c_{s1}\left[\dot{z}_f(t) - \ell_f\dot{\theta}(t) - \dot{z}_{t1}(t)\right] \\ &- c_{s2}\left[\dot{z}_f(t) + \ell_r\dot{\theta}(t) + \ell_{sl}\dot{\phi}(t) - \dot{z}_{t2}(t)\right] \\ &- c_{s3}\left[\dot{z}_f(t) + \ell_r\dot{\theta}(t) - \ell_{sr}\dot{\phi}(t) - \dot{z}_{t3}(t)\right] \\ &- c_{t1}\left[\dot{z}_f(t) - \dot{z}_{t1}(t)\right] - c_{t2}\left[\dot{z}_f(t) - \dot{z}_{t2}(t)\right] \\ &- c_{t3}\left[\dot{z}_f(t) - \dot{z}_{t3}(t)\right] + F_1(t) + F_2(t) \\ &+ F_3(t). \end{aligned} \tag{22}$$

For the vertical motion of the pilot's seat,

$$\begin{aligned} m_s\ddot{z}_s(t) = &-k_{fs}\left[z_s(t) - z_f(t) + \ell_{sf}\theta(t) - \ell_{ss}\phi(t)\right] \\ &- k_{sp}\left[z_s(t) - z_p(t)\right] \\ &- c_{fs}\left[\dot{z}_s(t) - \dot{z}_f(t) + \ell_{sf}\dot{\theta}(t) - \ell_{ss}\dot{\phi}(t)\right] \\ &- c_{sp}\left[\dot{z}_s(t) - \dot{z}_p(t)\right] \end{aligned} \tag{23}$$

For the vertical motion of the pilot's pelvis,

$$\begin{aligned} m_p\ddot{z}_p(t) = &-k_{sp}\left[z_p(t) - z_s(t)\right] - k_{pl}\left[z_p(t) - z_l(t)\right] \\ &- k_{pu}\left[z_p(t) - z_u(t)\right] \\ &- c_{sp}\left[\dot{z}_p(t) - \dot{z}_s(t)\right] - c_{pl}\left[\dot{z}_p(t) - \dot{z}_l(t)\right] \\ &- c_{pu}\left[\dot{z}_p(t) - \dot{z}_u(t)\right]. \end{aligned} \tag{24}$$

For the vertical motion of the pilot's lower torso,

$$\begin{aligned} m_l\ddot{z}_l(t) = &-k_{pl}\left[z_l(t) - z_p(t)\right] - k_{lu}\left[z_l(t) - z_u(t)\right] \\ &- c_{pl}\left[\dot{z}_l(t) - \dot{z}_p(t)\right] - c_{lu}\left[\dot{z}_l(t) - \dot{z}_u(t)\right]. \end{aligned} \tag{25}$$

For the vertical motion of the pilot's upper torso,

$$\begin{aligned} m_u\ddot{z}_u(t) = &-k_{pu}\left[z_u(t) - z_p(t)\right] - k_{lu}\left[z_u(t) - z_l(t)\right] \\ &- k_{uh}\left[z_u(t) - z_h(t)\right] \\ &- c_{pu}\left[\dot{z}_u(t) - \dot{z}_p(t)\right] - c_{lu}\left[\dot{z}_u(t) - \dot{z}_l(t)\right] \\ &- c_{uh}\left[\dot{z}_u(t) - \dot{z}_h(t)\right]. \end{aligned} \tag{26}$$

For the vertical motion of the pilot's head,

$$\begin{aligned} m_h\ddot{z}_h(t) = &-k_{uh}\left[z_h(t) - z_u(t)\right] \\ &- c_{uh}\left[\dot{z}_h(t) - \dot{z}_u(t)\right]. \end{aligned} \tag{27}$$

The above equations of motions can be written in the matrix form as

$$M_s\ddot{q}(t) + C_s\dot{q}(t) + K_s q(t) = F_s u(t) + E_s w(t), \quad (28)$$

where $q(t)$ is the generalized coordinates, $u(t)$ is the control force, $F_s \in \Re^{n\times m}$ gives the location of the controller, $w(t) \in \Re^p$ is the disturbance input, and $E_s \in \Re^{n\times p}$ is a matrix that weights the disturbances. Finally, $M_s, C_s, K_s \in \Re^{n\times n}$ are the mass, damping, and stiffness matrices of the modelled aircraft system, respectively. These matrices are given in Appendix.

Using the definition $x(t) = \begin{bmatrix} q(t) & \dot{q}(t) \end{bmatrix}^T$, system (28) can be expressed in state space form as

$$\dot{x}(t) = Ax(t) + B_1 w(t) + B_2 u(t), \quad (29)$$

where

$$A = \begin{bmatrix} 0 & I \\ -M_s^{-1}K_s & -M_s^{-1}C_s \end{bmatrix},$$
$$B_1 = \begin{bmatrix} 0 \\ M_s^{-1}E_s \end{bmatrix}, \quad (30)$$
$$B_2 = \begin{bmatrix} 0 \\ M_s^{-1}F_s \end{bmatrix}$$

and $w(t) = \begin{bmatrix} z_{r1}(t) & z_{r2}(t) & z_{r3}(t) & \dot{z}_{r1}(t) & \dot{z}_{r2}(t) & \dot{z}_{r3}(t) \end{bmatrix}^T$ is the vector of disturbances and $u(t) = \begin{bmatrix} F_1(t) & F_2(t) & F_3(t) \end{bmatrix}^T$ is the vector of control inputs.

3. Controller Design

LMI based controller design has received considerable attention in recent years [24–26]. In this paper, to improve system performance, an optimal observer based H_2 controller having pole location constraints is designed. Based on the integrated model, first an optimal full state feedback controller could be designed to improve the pilot's taxiing performance and essential safety requirements. However, it is well known that full sate feedback approach assumes that all the state variables belonging to the full aircraft system having active landing gears and pilot body are available for measurement. The assumption is questionable, when states of the biodynamic pilot body model are considered. In particular, the lower torso, upper torso, and head displacements and velocities are not practically measurable. Therefore, a full state feedback optimal controller is not suitable to improve active landing gear performance on pilot's comfort and aircraft safety during taxiing. On the other hand, dynamic output feedback controller could be implemented to solve the unmeasurable states problem; however it is an expensive and difficult solution when the model order is increased by adding frequency weighting performance filters [27]. Therefore, in this study an optimal observer based H_2 controller having pole location constraints which is less expensive and more practically reliable is applied to the active landing gear system to fulfill the desired performance requirements. The main control objectives are guaranteed asymptotic stability of the closed loop system and disturbance attenuation in the sense of H_2 norm. First, solvability conditions for optimal observed based H_2 state feedback controller are expressed in terms of a set of LMIs. Then, additional LMI constraints are added to place the closed loop poles into the desired domains in complex plane.

Consider an open-loop state space system given by

$$\begin{aligned} \dot{x}(t) &= Ax(t) + B_1 w(t) + B_2 u(t), \\ z(t) &= C_1 x(t) + D_{11} w(t) + D_{12} u(t), \\ y(t) &= C_2 x(t) + D_{21} w(t) + D_{22} u(t), \end{aligned} \quad (31)$$

where $x(t) \in \Re^n$ is the state vector, $u(t) \in \Re^m$ is the control inputs vector, $w(t) \in \Re^p$ is the disturbance inputs vector acting on the system, $z(t) \in \Re^c$ is the controlled outputs vector, and $y(t) \in \Re^q$ is the measured outputs vector. Then, $A \in \Re^{n\times n}$, $B_1 \in \Re^{n\times p}$, and $B_2 \in \Re^{n\times m}$ are known, real, constant state differential equation matrices and $C_1 \in \Re^{c\times n}$, $D_{11} \in \Re^{c\times p}$, and $D_{12} \in \Re^{c\times m}$ are the matrices to represent controlled outputs and $C_2 \in \Re^{q\times n}$, $D_{21} \in \Re^{q\times p}$, and $D_{22} \in \Re^{q\times m}$ denote the measured outputs with appropriate dimensions.

Rest of this section is organized as follows. Section 3.1 describes the synthesis of optimal state feedback H_2 controller having pole location constraints by the use of LMI regions. Thereafter, design of a full order optimal H_2 observer is given in Section 3.2. Finally, observer based state feedback optimal controller design is constructed in Section 3.3.

Subscript "c" stands for scalar variables or unknown variables related to state feedback controller and subscript "o" stands for the full order observer.

3.1. Optimal State Feedback Controller Design Having Pole Location Constraints. In this section, it is assumed that all the state variables are available for measurement. Hence, a state feedback control law

$$u(t) = Kx(t), \quad (32)$$

which is a linear function of state vector, can be constructed. Here, $K \in \Re^{m\times n}$ is the state feedback controller gain. Then, the closed loop system can be written using (31) and (32) as

$$\begin{aligned} \dot{x}(t) &= (A + B_2K)x(t) + B_1 w(t), \\ z(t) &= (C_1 + D_{12}K)x(t) + D_{11} w(t). \end{aligned} \quad (33)$$

An optimal state feedback controller must ensure stability and specified performance against disturbances at the same time. In the presence of exogenous inputs such as disturbances, minimization of H_2 norm is one of the well accepted performance specifications [28]. Here, $\|T_{zw}\|_2$ stands for H_2 norm of the transfer function matrices from disturbances $w(t)$ to controlled outputs $z(t)$ for the closed loop system (33).

Lemma 1 presents a full state feedback H_2 controller design.

Lemma 1 (see [29]). *For a given nonnegative scalar η_c, the closed loop system (33) is asymptotically stable with H_2 norm less than η_c, if there exist positive-definite symmetric matrix $X_c \in \mathfrak{R}^{n\times n}$ and a rectangular matrix $F_c \in \mathfrak{R}^{m\times n}$ subject to*

$$\begin{aligned} &trace\left(Q_c\right) < \eta_c^2, \\ &\begin{bmatrix} Q_c & C_1X_c + D_{12}F_c \\ X_cC_1^T + F_c^TD_{12}^T & X_c \end{bmatrix} \succ 0, \\ &AX_c + B_2F_c + X_cA + F_c^TB_2^T + B_1^TB_1 \prec 0. \end{aligned} \tag{34}$$

Then, the control law $u(t) = Kx(t) = F_cX_c^{-1}x(t)$ is a full state feedback H_2 controller associated with H_2 norm less than η_c.

It is well known that the transient response of a linear system is related to location of its poles in complex plane. Therefore controller design with constraints on closed loop pole locations can ensure satisfactory transient response. Establishing a lower bound for decay rate and an upper bound for damping ratio can be described as domains in complex plane as follows:

$$\begin{aligned} H_{\tau_c} &= \left\{x + jy \mid x < -\tau_c < 0\right\}, \\ H_\theta &= \left\{x + jy \mid \left|y\right| < x\tan\theta_c < 0\right\}, \end{aligned} \tag{35}$$

where τ_c is the positive real number that restricts the real part of closed loop poles and θ_c is the value of the angle to prescribe desired damping ratio as $\cos(\theta_c)$. Any domain in complex plane can be represented as a LMI region, if there exist a symmetric matrix $G \in \mathfrak{R}^{d\times d}$ and unstructured matrix $M \in \mathfrak{R}^{d\times d}$ such that

$$D_{(G,M)} = \left\{s \in C \mid G + sM + \bar{s}M^T \prec 0\right\}, \tag{36}$$

where s is a complex number and superscript $\bar{s}$ stands for complex conjugate of s. Then, $D_{(G,M)}$ is called an LMI region [30]. Hence, closed loop pole location constraints can be formulated in LMI approach by Lemma 2.

Lemma 2 (see [30]). *For a given LMI region $D_{(G,M)}$ associated with G and M, a matrix $N \in R^{n\times n}$ is $D_{(G,M)}$ stable if and only if there exists a symmetric positive-definite matrix $P \in \mathfrak{R}^{n\times n}$ which satisfies*

$$G \otimes P + M \otimes (NP) + M^T \otimes (NP)^T \prec 0, \tag{37}$$

where $\otimes$ is the Kronecker product.

In the light of Lemma 2, to place the poles of the $A + B_2K$ into a LMI region described by (35),

$$\begin{aligned} G_{\tau_c} &= 2\tau_c, \\ M_{\tau_c} &= 1, \\ G_{\theta_c} &= 0_{2\times 2}, \\ M_{\theta_c} &= \begin{bmatrix} \sin\theta_c & \cos\theta_c \\ -\cos\theta_c & \sin\theta_c \end{bmatrix} \end{aligned} \tag{38}$$

can be used [30, 31]. Then, the matrices (38) are substituted into (37) and as follows and one obtains

$$\begin{aligned} &2\tau_cP + AP + B_2W_c + PA^T + W_c^TB_2^T \prec 0, \\ &\begin{bmatrix} \left(AP + PA^T + B_2W_c + W_c^TB_2^T\right)\sin\theta_c & \left(PA^T - AP_c + W_cB_2^T - B_2W_c\right)\cos\theta_c \\ \left(AP - PA^T + B_2W_c - W_c^TB_2\right)\cos\theta_c & \left(AP + PA^T + B_2W_c + W_cB_2^T\right)\sin\theta_c \end{bmatrix} \prec 0. \end{aligned} \tag{39}$$

Here, a change of variable $W_c = KP$ is performed to tackle the bilinear matrix inequality problem. Hence, state feedback controller with pole location constraints can be calculated as $K = W_cP^{-1}$ by the solution of (39).

By assuming that $K = W_cP^{-1} = F_cX_c^{-1}H_2$ controller with pole location constraints can be designed. $F_c = W_c$ and $X_c = P$ are compulsory assumptions, since the constraint $W_cY_c^{-1} = F_cX_c^{-1}$ is nonconvex. Consequently, computation of a H_2 state feedback controller gain with pole location constraints can be performed by the following theorem.

Theorem 3. *For given positive scalars η_c, τ_c, and θ_c, the closed loop system (33) is asymptotically stable with H_2 norm less than η_c and closed loop poles are shifted to the left side of $-\tau_c$ with a damping ratio which is smaller than $\cos(\theta_c)$, if there exist positive-definite symmetric matrices $X_c \in \mathfrak{R}^{n\times n}$ and $Q_c \in \mathfrak{R}^{c\times c}$ and a rectangular matrix $F_c \in \mathfrak{R}^{m\times n}$ subject to*

$$\begin{aligned} &AX_c + B_2F_c + X_cA^T + F_c^TB_2^T + B_1^TB_1 \prec 0, \\ &\begin{bmatrix} Q_c & C_1X_c + D_{12}F_c \\ X_cC_1^T + F_c^TD_{12}^T & X_c \end{bmatrix} \succ 0, \\ &trace\left(Q\right) < \eta_c, \end{aligned}$$

$$2\tau_c X_c + AX_c + X_c A^T + B_2 F_c + F_c^T B_2^T \prec 0,$$

$$\begin{bmatrix} \left(AX_c + X_c A^T + B_2 F_c + Y_c F_c^T\right)\sin\theta_c & \left(X_c A^T - AX_c + F_c B_2^T - B_2 F_c\right)\cos\theta_c \\ \left(AX_c - X_c A^T + B_2 F_c - Y_c F_c^T\right)\cos\theta_c & \left(AX_c + X_c A^T + B_2 F_c + F_c B_2^T\right)\sin\theta_c \end{bmatrix} \prec 0. \tag{40}$$

Then, the control law $u(t) = Kx(t) = F_c X_c^{-1} x(t)$ is state feedback H_2 controller having pole location constraints. If the minimization of η_c is considered, the resulting state feedback controller is an optimal H_2 controller.

3.2. Optimal Full Order Observer Design Having Pole Location Constraints. In this section, LMI based optimal full order observer design is presented. It is well known that state feedback control approach assumes that all states are available for feedback. However, it is not the case in many real life applications. Thus, observer design is a very important issue and needed in many applications. An observer is another dynamical system which aims to observe the states which are unavailable for measurement. Therefore, a full order observer is given in the form of

$$\begin{aligned} \dot{\widehat{x}}(t) &= A\widehat{x}(t) + B_2 u(t) + L\left(\widehat{y}(t) - y(t)\right), \\ \widehat{y}(t) &= C_2 \widehat{x}(t) + D_{22} u(t), \end{aligned} \tag{41}$$

where $\widehat{x}(t)$ is the state observation vector and $\widehat{y}(t)$ is the observer output vector. Finally, $L \in \mathfrak{R}^{n\times q}$ is the observer gain. Observation error and dynamics are defines as

$$\begin{aligned} e(t) &= x(t) - \widehat{x}(t), \\ \dot{e}(t) &= \left(A + LC_2\right) e(t) + \left(B_1 + LD_{21}\right) w(t), \\ \widehat{z}(t) &= C_3 e(t). \end{aligned} \tag{42}$$

An optimal full order observer design problem can be stated as making the observation error asymptotically stable and least sensitive to the disturbance $w(t)$. Here $\widehat{z}(t) \in \mathfrak{R}^k$ and $C_3 \in \mathfrak{R}^{k\times n}$ are the related vector and matrix to choose which observation errors must be less affected by disturbances. Thereafter, full order H_2 observer gain can be computed as given in Lemma 4.

Lemma 4 (see [29]). *For a given nonnegative scalar η_o, observation error (42) is asymptotically stable with H_2 norm less than η_o, if there exist symmetric positive-definite matrix $X_o \in \mathfrak{R}^{n\times n}$ and a rectangular matrix $F_o \in \mathfrak{R}^{n\times q}$ subject to*

$$\begin{aligned} &trace\left(Q_o\right) < \eta_o^2, \\ &\begin{bmatrix} X_o A + F_o C_2 + A^T X_o + C_2^T F_o^T & X_o B_1 + F_o D_{21} \\ B_1^T X_o + D_{21}^T F_o^T & -I \end{bmatrix} \prec 0, \\ &\begin{bmatrix} Q_o & C_3 \\ C_3^T & X_o \end{bmatrix} \succ 0 \end{aligned} \tag{43}$$

Then, $L = X_o^{-1} F_o$ is a full order H_2 observer gain.

In order to improve observation performance, pole location constraints with the LMI regions are added to the full order observer design. By the use of Lemma 2 which is given in Section 3.1, poles of the observation error dynamics (42) can be placed into a LMI region with guarantee of decay rate and damping ratio associated with τ_o and θ_o, as given in

$$2\tau_o Y_o + Y_o A + W_o C_2 + A^T Y_o + C_2^T W_o^T \prec 0,$$

$$\begin{bmatrix} \left(Y_o A + A^T Y_o + W_o C_2 + C_2^T W_o^T\right)\sin\theta_o & \left(A^T Y_o - Y_o A + C_2^T W_o^T - W_o C_2\right)\cos\theta_o \\ \left(Y_o A - A^T Y_o + W_o C_2 - C_2^T W_o^T\right)\cos\theta_o & \left(Y_o A + A^T Y_o + W_o C_2 + C_2^T W_o^T\right)\sin\theta_o \end{bmatrix} \prec 0, \tag{44}$$

where $Y_o = P^{-1}$ and $W_o = Y_o L$. Hence, by assuming that $L = X_o^{-1} F_o = Y_o^{-1} W_o$ an optimal full order H_2 observer having pole location constraints can be designed. Since, $X_o^{-1} F_o = Y_o^{-1} W_o$ is not a convex constraint, $F_o = W_o$ and $X_o = Y_o$ are compulsory assumptions. Consequently, full order observer design procedure is formulated in Theorem 5.

Theorem 5. *For given positive scalars η_o, τ_o, and θ_o, observation error (42) is asymptotically stable with H_2 norm less than η_o and observer poles are shifted to the left side of $-\tau_o$ with a damping ratio which is smaller than $\cos(\theta_o)$, if there exist positive-definite symmetric matrix $X_o \in \mathfrak{R}^{n\times n}$ and a rectangular matrix $F_o \in \mathfrak{R}^{n\times q}$ subject to*

$$trace\left(Q_o\right) < \eta_o^2,$$

$$\begin{bmatrix} X_o A + F_o C_2 + A^T X_o + C_2^T F_o^T & X_o B_1 + F_o D_{21} \\ B_1^T X_o + D_{21}^T F_o^T & -I \end{bmatrix} \prec 0,$$

$$\begin{bmatrix} Q_o & C_3 \\ C_3^T & X_o \end{bmatrix} \succ 0,$$

$$2\tau_o X_o + X_o A + S_o C_2 + A^T X_o + C_2^T S_o^T \prec 0,$$

$$\begin{bmatrix} \left(X_o A + A^T X_o + F_o C_2 + C_2^T F_o^T\right)\sin\theta_o & \left(A^T X_o - X_o A + C_2^T F_o^T - F_o C_2\right)\cos\theta_o \\ \left(X_o A - A^T X_o + F_o C_2 - C_2^T F_o^T\right)\cos\theta_o & \left(X_o A + A^T X_o + F_o C_2 + C_2^T F_o^T\right)\sin\theta_o \end{bmatrix} \succ 0. \tag{45}$$

Then, η_o is an upper bound in terms of the H_2 norm for the error dynamics (42), from $w(t)$ to $\widetilde{z}(t)$ for all ≥ 0, and the observer gain is $L = X_o^{-1}F_o$. If the minimization of η_o is considered, the resulting observer is an optimal full order H_2 observer.

3.3. Construction of Observer Based Optimal Controller. In this section, observer based controller structure is introduced. A full order observer can be rewritten as

$$\dot{\widehat{x}}(t) = \left(A + LC_2\right)\widehat{x}(t) + \left(B_2 + LD_{22}\right)u(t) - Ly(t), \tag{46}$$

where computation of L is formulated by Theorem 5. Here, a full order observer (46) is a dynamical system which takes control input $u(t)$ and measured outputs $y(t)$ as inputs to produce the estimation of the state vector $\widehat{x}(t)$. By combining the state feedback gain matrix K which can be calculated with Theorem 3, an observer based controller

$$\begin{aligned} \dot{\widehat{x}}(t) &= \left(A + LC_2\right)\widehat{x}(t) + \left(B_2 + LD_{22}\right)u(t) - Ly(t), \\ u(t) &= K\widehat{x}(t), \end{aligned} \tag{47}$$

is obtained. Integrated structure of the state feedback and observer is depicted in Figure 2.

4. Numerical Simulation Study

In this section, extensive numbers of simulations are carried out to verify the effectiveness and applicability of the proposed controller in reducing the effect of runway irregularities on the modeled full aircraft system and to improve ride quality during taxiing. The full aircraft system parameters used in the simulations are given in Table 1, where the full aircraft model with landing gears parameters is borrowed from [22], and the seat suspension and biodynamic pilot body parameters are discussed in [23, 32].

In order to demonstrate proposed controller performance, two typical runway profiles are used as disturbance input which are applied to the aircraft tires. Bump type road profile is considered first to reveal the transient response characteristics which is given by

$$z_{r1}(t) = \begin{cases} 0.04\left(1 - \cos\left(\omega t\right)\right), & 0.2 \leq t \leq 1 \\ 0, & \text{otherwise,} \end{cases}$$

$$z_{r2}(t) = \begin{cases} 0.1\left(1 - \cos\left(\omega t\right)\right), & 5 \leq t \leq 5.8 \\ 0, & \text{otherwise,} \end{cases}$$

$$z_{r3}(t) = \begin{cases} 0.06\left(1 - \cos\left(\omega t\right)\right), & 2.6 \leq t \leq 3.4 \\ 0, & \text{otherwise,} \end{cases} \tag{48}$$

where duration of each impulse is 0.8 s and the frequency ω is 7.85 rad/s [22]. Then, very poor random runway profile is used as the worst case disturbance input. The runway disturbance is generated by a shaping filter method which is described in [22, 33, 34]. It is typically specified as random process with a ground displacement Power Spectral Density (PSD) of

$$S(\omega) = \frac{2\alpha V\sigma^2}{\omega^2 + \alpha^2 V^2}, \tag{49}$$

where σ^2 denotes the runway roughness variance (m^2), V is the aircraft longitudinal speed (m/s), and α depends on the type of runway surface (rad/m). Hence, if the aircraft runs with the constant speed, the PSD (49) and the random runway profile signal may be obtained as the output of a first-order linear filter expressed as

$$\dot{z}_r(t) = -\alpha V z_r(t) + \omega(t), \tag{50}$$

where $\omega(t)$ is a white noise process with the spectral density $S(\omega)$. The road roughness standard deviations for various runway types are given in Table 2 [22].

In this study, runway excitation with E grade very poor random road profile has been considered for the value of longitudinal speed V that is 50 m/s. The modelled bump and very poor random runway disturbances are shown in Figure 3.

In this section, first, an observer based optimal state feedback controller is designed for active vibration control of full aircraft system having active landing gears and biodynamic pilot body. Then, to compare the control performance and show the effectiveness of the proposed observer based optimal state feedback controller with classical LQR controller, the LQR is designed and simulation studies are performed. All the simulations and computations are accomplished using Matlab with Simulink. For the solution of the resulting LMIs, Yalmip parser and Sedumi solver are used [35, 36].

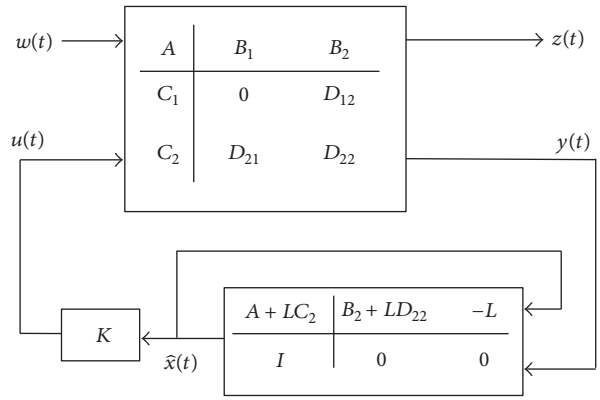

Figure 2: Structure of the observer based controller.

In order to ensure the responses within permissible limits for the essential safety and comfort requirements, the controlled output vector $z(t)$ is constructed as

$$z(t) = \left[r_1\phi(t) \;\; r_2\theta(t) \;\; r_3 z_{\mathrm{f}}(t) \;\; r_4 z_{\mathrm{h}}(t) \;\; r_5 d_{\mathrm{s1}}(t) \;\; r_6 d_{\mathrm{s2}}(t) \;\; r_7 d_{\mathrm{s3}}(t)\right]^T, \tag{51}$$

where $d_{\mathrm{s1}}(t)$, $d_{\mathrm{s2}}(t)$, and $d_{\mathrm{s3}}(t)$ are suspension strokes and previously given in (7), (8), and (9). In addition, each scalar r_i $(i = 1, 2, \ldots, 7)$ given in (51) corresponds to weighting coefficients and their values are given in Table 1. The controlled outputs vector $z(t)$ is described in matrix form as follows:

$$z(t) = C_1 x(t) + D_{11} w(t) + D_{12} u(t), \tag{52}$$

where C_1 is the controlled outputs state matrix, D_{11} is the control input matrix for the controlled outputs, and D_{12} is the disturbance input scaling matrix for the controlled outputs.

To guarantee asymptotic convergence of observed state variables with an optimal observation performance, appropriate measured outputs must be chosen. In the observer design measured outputs are selected as

$$\begin{aligned} &y(t) \\ &= \left[d_{\mathrm{s1}}(t) \;\; d_{\mathrm{s2}}(t) \;\; d_{\mathrm{s3}}(t) \;\; z_{\mathrm{s}}(t) - z_{\mathrm{f}}(t) \;\; \phi(t) \;\; \theta(t) \;\; z_{\mathrm{f}}(t) \;\; z_{\mathrm{s}}(t) \;\; \dot{\phi}(t) \;\; \dot{\theta}(t) \;\; \cdots \;\; \dot{z}_{\mathrm{f}}(t) \;\; \dot{z}_{\mathrm{s}}(t) \;\; \dot{d}_{\mathrm{s1}}(t) \;\; \dot{d}_{\mathrm{s2}}(t) \;\; \dot{d}_{\mathrm{s3}}(t) \;\; \ddot{z}_{\mathrm{t1}} \;\; \ddot{z}_{\mathrm{t2}} \;\; \ddot{z}_{\mathrm{t3}} \;\; \ddot{\phi}(t) \;\; \ddot{\theta}(t) \;\; \ddot{z}_{\mathrm{f}}(t) \;\; \ddot{z}_{\mathrm{s}}(t)\right]^T. \end{aligned} \tag{53}$$

The measured outputs vector $y(t)$ is described in matrix form as follows:

$$y(t) = C_2 x(t) + D_{21} w(t) + D_{22} u(t), \tag{54}$$

where C_2 is the measured outputs state matrix, D_{21} is the control input matrix for the measured outputs, and D_{22} is the disturbance input scaling matrix for the measured outputs.

In the light of Theorem 3, in order to achieve a minimum H_2 norm from $w(t)$ to $z(t)$ for all $t \geq 0$, one can solve the following optimization problem for the positive-definite symmetric matrices X_c and Q_c, and matrix F_c and positive scalar η_c,

$$\begin{aligned} &\min \quad \eta_c \\ &\text{s.t.} \quad (40). \end{aligned} \tag{55}$$

If the above optimization problem has a feasible solution, a state feedback optimal control law can be constructed as

$$u(t) = F_c X_c^{-1} x(t). \tag{56}$$

Applying Theorem 3 to this example, η_c is calculated as 28.6555. To improve control performance, the closed loop poles are shifted to the left side of $\tau_c = -15$ and damping ratios of each pole are enforced to be less than 0.17 which is the maximum damping ratio value of the open-loop poles.

Then, Theorem 5 is used to construct the observer based controller. To improve observation performance, the observer poles are shifted to the left side of $\tau_{o1} = -10$ and right side of $\tau_{o2} = -200$ with damping ratios less than 0.7. In order to achieve a minimum H_2 norm from $w(t)$ to $\widehat{z}(t)$ for all $t \geq 0$, one can solve the following optimization problem

Table 1: The parameter values of the proposed full aircraft model and the numerical values of controlled variables coefficients.

Symbol	Value	Units
m_{t1}	130	[kg]
m_{t2}	260	[kg]
m_{t3}	260	[kg]
I_x	65×10^3	[kgm^2]
I_y	100×10^3	[kgm^2]
m_f	22×10^3	[kg]
m_s	15	[kg]
m_p	36	[kg]
m_l	5.5	[kg]
m_u	15	[kg]
m_h	4.17	[kg]
k_{t1}	1.59×10^6	[N/m]
k_{t2}	1.59×10^6	[N/m]
k_{t3}	1.59×10^6	[N/m]
k_{s1}	6.73×10^5	[N/m]
k_{s2}	4.08×10^5	[N/m]
k_{s3}	4.08×10^5	[N/m]
k_{fs}	31×10^3	[N/m]
k_{sp}	49340	[N/m]
k_{pl}	2×10^4	[N/m]
k_{pu}	144×10^3	[N/m]
k_{lu}	1×10^4	[N/m]
k_{uh}	166990	[N/m]
c_{t1}	4066	[Ns/m]
c_{t2}	4066	[Ns/m]
c_{t3}	4066	[Ns/m]
c_{s1}	1.43×10^5	[Ns/m]
c_{s2}	6.25×10^5	[Ns/m]
c_{s3}	6.25×10^5	[Ns/m]
c_{fs}	830	[Ns/m]
c_{sp}	2475	[Ns/m]
c_{pl}	330	[Ns/m]
c_{pu}	909.1	[Ns/m]
c_{lu}	200.00	[Ns/m]
c_{uh}	310.00	[Ns/m]
ℓ_f	7.76	[m]
ℓ_r	1.94	[m]
ℓ_{sl}	3.8425	[m]
ℓ_{sr}	3.8425	[m]
ℓ_{sf}	7	[m]
ℓ_{ss}	0.5	[m]
r_1	450	—
r_2	450	—
r_3	150	—
r_4	1	—
r_5	50	—
r_6	50	—
r_7	50	—

Table 2: Road roughness and standard deviation [22].

Road class	σ (10^{-3} m)	$\phi(\Omega_0)$ (10^{-6}m^3), $\Omega_0 = 1$	α (rad/m)
A (very good)	2	1	0.127
B (good)	4	4	0.127
C (average)	8	16	0.127
D (poor)	16	64	0.127
E (very poor)	32	256	0.127

for the positive-definite symmetric matrices Z_o and Q_o and matrix S_o and positive scalar η_o,

$$\begin{aligned} &\min \quad \eta_o \\ &\text{s.t.} \quad (45)\,. \end{aligned} \tag{57}$$

If the above optimization problem has a feasible solution, a full order optimal observer gain is computed as

$$L = X_o^{-1} F_o \tag{58}$$

and η_o is calculated as 0.2121. Then, the observer based controller gains can be calculated by the use of (56) and (58) as explained in Section 3.3. For brevity, developed observer based optimal state feedback controller is henceforth denoted as Controller 1.

To validate and compare the control performance of proposed observer based controller with classical LQR controller, the design equations for a LQR controller can be obtained as in Theorem 6.

Theorem 6 (see [37]). *LQR controller design problem is to find an optimal full state feedback control law that minimizes the quadratic cost function*

$$J = \int_0^\infty x^T(t)\, Qx(t) + u^T(t)\, Ru(t)\, dt, \tag{59}$$

where performance weighting matrices are symmetric and positive semidefinite $Q = Q^T \geq 0$ and a symmetric positive-definite matrix $R = R^T > 0$. Solution of Algebraic Riccati Equation (ARE)

$$SA + A^T S + Q + SB_2 R^{-1} B_2^T S = 0 \tag{60}$$

provides the optimal solution. Then, the LQR control law can be obtained as

$$u(t) = -R^{-1} B_2^T S x(t)\,. \tag{61}$$

The performance weighting matrices of the LQR controller are constructed for active vibration control of full aircraft system as

$$\begin{aligned} Q &= \operatorname{diag}\left(0_{3\times 11}, 25, 15, 5, 0_{4\times 11}, 5, 0_{1\times 11}\right), \\ R &= \operatorname{diag}(400, 40, 40)\,. \end{aligned} \tag{62}$$

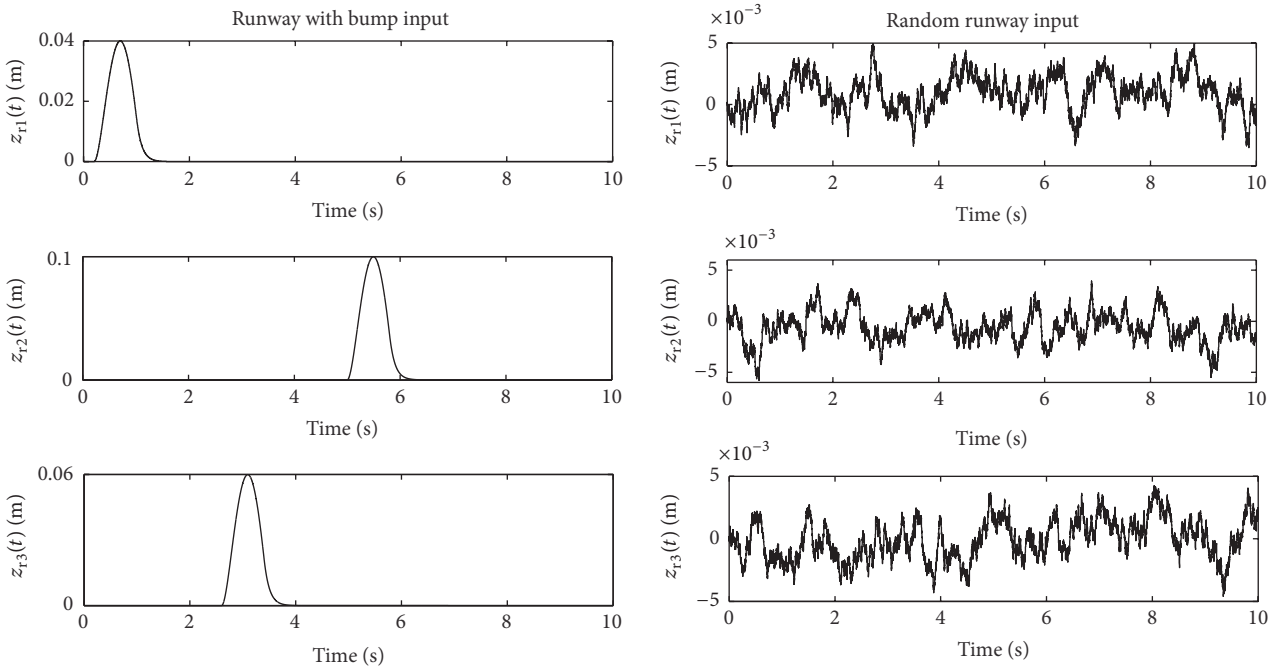

Figure 3: Bump and random runway disturbance inputs.

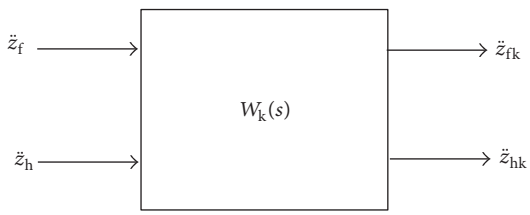

Figure 4: Block diagram of the frequency weighting.

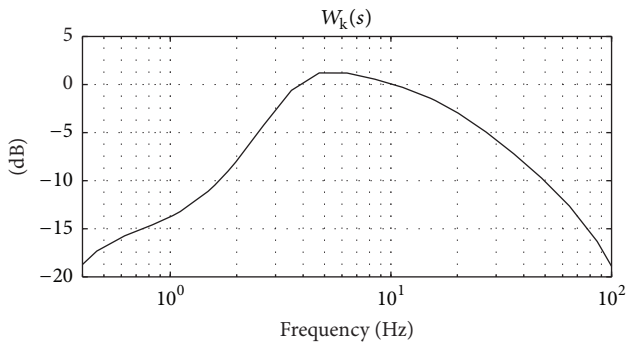

Figure 5: ISO2631 frequency weighting filter.

By the use of Theorem 6, LQR control law can be easily calculated. For brevity, designed LQR controller is henceforth denoted as Controller 2.

It is well known that the safety and comfort are the essential performance requirements for the active landing gear design problem. The safety of the aircraft mainly depends on the suspension stroke and tire deflection responses, while the comfort level of the pilot depends on the pilot's head acceleration response. Ride comfort is known to be frequency sensitive. It is defined by ISO2631-1; humans are most sensitive in the frequency band 4–10 Hz for the vertical direction. Therefore, frequency weighting operation must be performed with band pass filter $W_k(s)$ on the vertical acceleration time histories as shown in Figure 4 [38, 39].

Band pass filter $W_k(s)$ coefficients are borrowed from [38], to weight the acceleration time histories in the vertical direction. Frequency response of the band pass filter is shown in Figure 5.

It is apparently seen that the frequency band 4–10 Hz is the most sensitive region for humans as previously stated. Figure 6 shows the time responses of roll, pitch acceleration of fuselage, and weighted vertical acceleration of pilot's head and fuselage, respectively, for both controlled and uncontrolled cases. When the acceleration response plots of considered aircraft system with uncontrolled and controlled cases are compared, a superior improvement in the mitigation of the maximum amplitude values is obtained by the use of proposed Controller 1 and Controller 2.

The corresponding peak values of roll, pitch acceleration responses of fuselage, and weighted vertical pilot's head and fuselage acceleration response are compared in Table 3 for bump and E grade very poor random road disturbance inputs, respectively.

As it can be observed from Table 3, Controller 1 achieves good control performance on ride comfort during taxiing in terms of the peak value of pilot head acceleration.

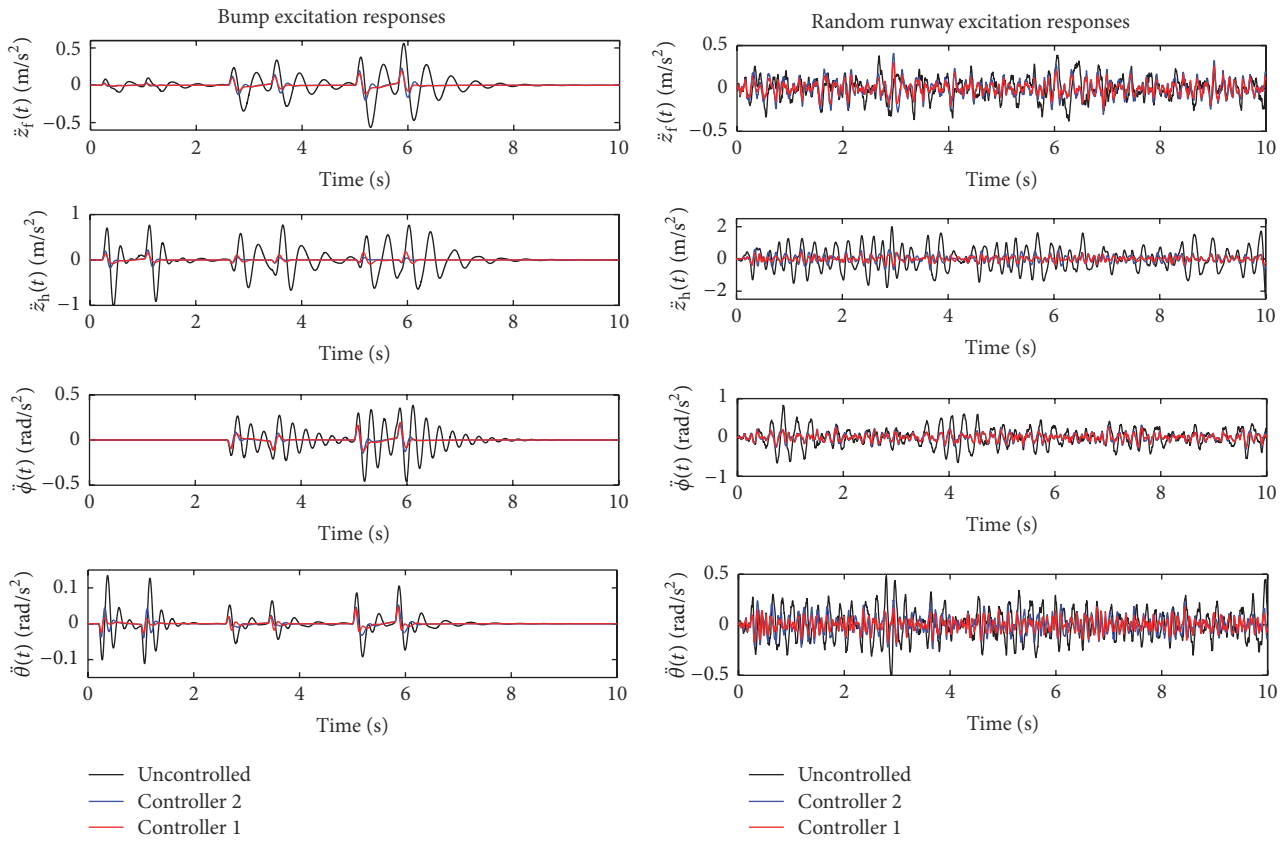

Figure 6: Controlled and uncontrolled acceleration time responses under bump and random runway excitation.

Table 3: Comparison of peak values of acceleration responses for both controlled and uncontrolled cases.

	Bump			Random		
	Passive	Controller 2	Controller 1	Passive	Controller 2	Controller 1
$\ddot{z}_{fk}(t)$	0.5654	0.2290	0.1939	0.3860	0.4077	0.3017
$\ddot{z}_{hk}(t)$	1.0303	0.2195	0.1782	2.4260	0.6801	0.4733
$\ddot{\phi}(t)$	0.6417	0.2766	0.3164	0.8143	0.3963	0.3406
$\ddot{\theta}(t)$	0.1874	0.0828	0.0667	0.6057	0.2958	0.2442

To validate and compare the control performance of proposed observer based controller with classical LQR controller, the peak values of the roll, pitch acceleration responses of fuselage, and weighted vertical pilot's head and fuselage acceleration responses are shown in Figure 7 for A grade (very good), B grade (good), C grade (average), D grade (poor), and E grade (very poor) road disturbance inputs.

Figure 7 demonstrates that a superior improvement in the attenuation of the maximum amplitude values is obtained by the use of Controller 1. Note that proposed Controller 1 largely reduces the pilot's head acceleration compared to Controller 2 and therefore achieves very successful taxiing performance.

The landing gear suspension stroke and tire deflection under bump and random runway excitation are compared for the controlled and uncontrolled cases in Figure 8. It is observed that the main safety requirements, which are the suspension stroke and road holding, are fulfilled by the proposed Controller 1 and Controller 2.

Additionally, to evaluate the proposed controller performance on different performance aspects using quantitative results, the peak values of landing gear suspension stroke and tire deflection responses are given in Table 4 for the controlled and uncontrolled cases. Table 4 reveals that designed Controller 1 has a satisfactory control performance and achieves a good trade-off, when the different performance requirements are considered.

Figure 9 demonstrates the change in control forces for Controller 1 and Controller 2 against bump and random

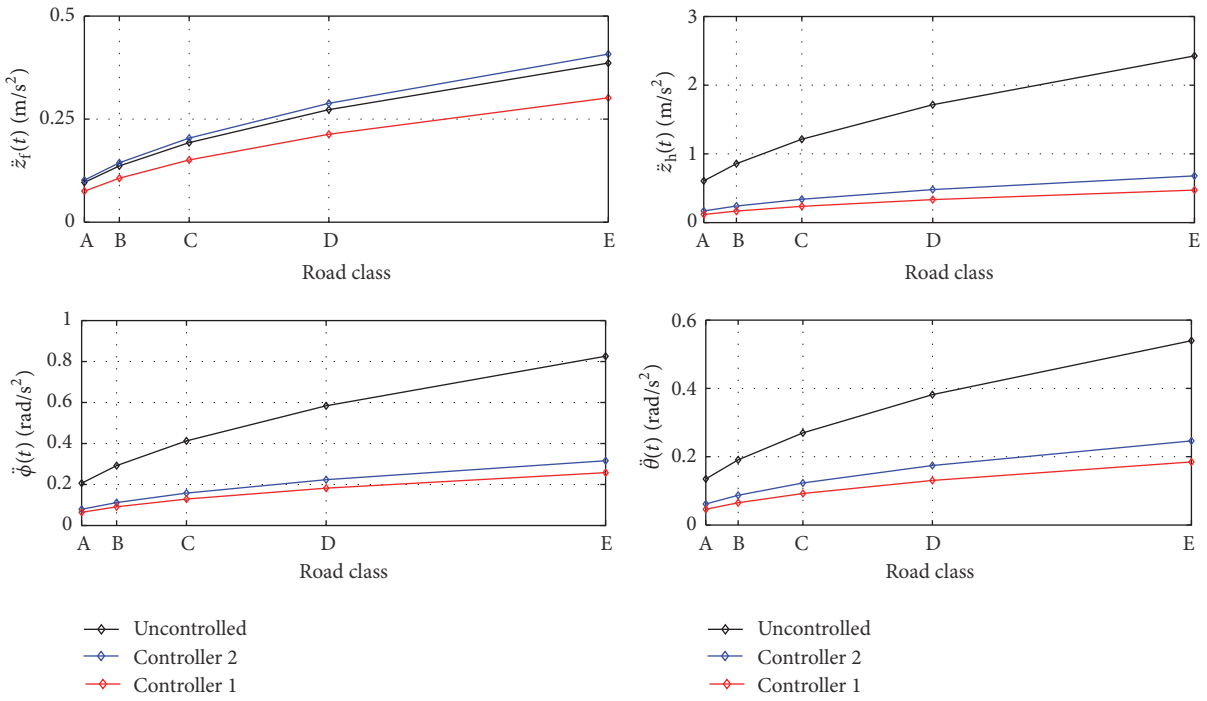

Figure 7: Peak values of acceleration responses under A grade, B grade C grade, D grade, and E grade road class disturbance inputs.

Table 4: Comparison of peak values of landing gear suspension stroke and tire deflection responses for both controlled and uncontrolled cases.

	Bump			Random		
	Passive	Controller 2	Controller 1	Passive	Controller 2	Controller 1
$d_{s1}(t)$	0.0857	0.0469	0.0471	0.0151	0.0083	0.0078
$d_{s2}(t)$	0.1250	0.1256	0.1436	0.0101	0.0087	0.0091
$d_{s3}(t)$	0.0850	0.0741	0.0849	0.0105	0.0053	0.0058
$z_{t1}(t) - z_{r1}(t)$	0.0033	0.0007	0.0008	0.0041	0.0028	0.0027
$z_{t2}(t) - z_{r2}(t)$	0.0100	0.0045	0.0041	0.0055	0.0037	0.0031
$z_{t3}(t) - z_{r3}(t)$	0.0093	0.0027	0.0024	0.0053	0.0032	0.0028

runway irregularities. In this figure, it is seen that the applied control forces could be produced for practical implementation.

Desired LMI regions and resulting closed loop pole locations obtained by Controller 1 and Controller 2 are shown in Figure 10. As it can be observed from Figure 10, all the closed loop poles are successfully placed in the desired LMI regions by Controller 1.

Figure 11 indicates the observation error and it is obvious from the responses that the unmeasurable states of the pilot's body are observed successfully.

Figure 12 shows the frequency responses of the bounce, roll, and pitch modes of fuselage and vertical of pilot's head, respectively, for both controlled and uncontrolled cases.

As expected, high gain responses belong to the uncontrolled system. It is obvious that all modes are successfully suppressed by the use of Controller 1 and Controller 2. Additionally, Controller 1 provides the least gains of system response over the frequency band 4–10 Hz, when compared with the uncontrolled system and Controller 2. Therefore, it is clearly seen that a superior improvement in the ride comfort is achieved by Controller 1.

Remark 7. As it can be observed from simulation results, designed Controller 1 and Controller 2 are both effective in reducing vibration amplitudes. In general, a full state feedback control law provides better control performance against an observer based control law. However, in this study, designed Controller 1 has better disturbance attenuation performance on the acceleration responses without a degradation on tire deflection which directly affects the road holding. Hence, maneuvering and braking responses

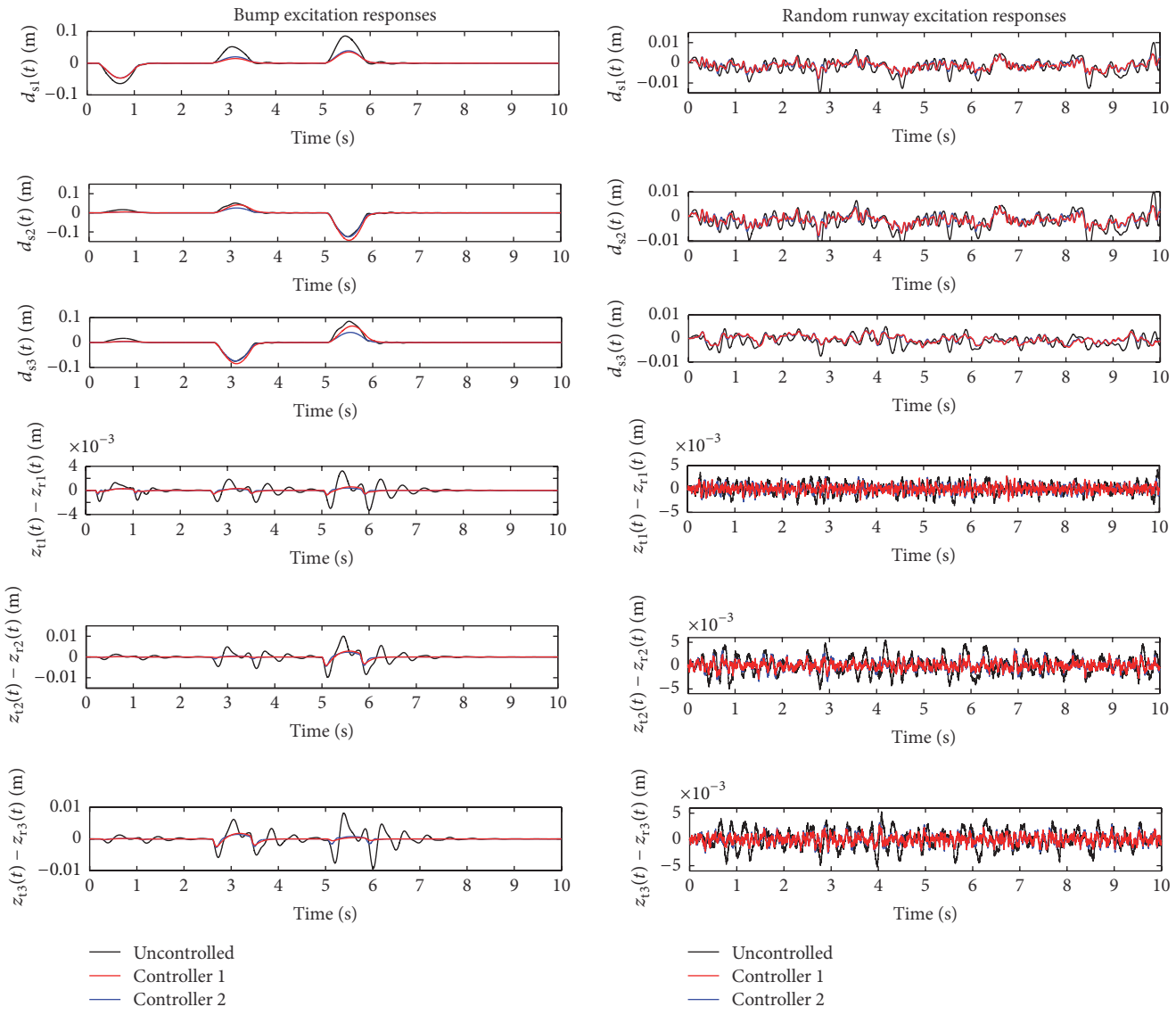

Figure 8: Controlled and uncontrolled bump and random runway responses on suspension stroke and tire deflection properties.

during the landing are expected to be improved. In addition, frequency responses reveal that Controller 1 has superior vibration mitigation performance over the frequency band 4–10 Hz which drastically influences the ride comfort [38]. Therefore, with this study, a simple easily realizable synthesis method is proposed to obtain observed based optimal control law for full aircraft system having active landing gears and biodynamic pilot body model under runway excitation.

5. Conclusions

This paper presents an approach for designing observer based optimal state feedback controller to attenuate vibrations that occurred in full aircraft system. Since the state variables of the pilot's body are not available for measurement, an observer based optimal controller design has been proposed. In order to improve controller performance, pole location constraints are included in the controller design process. The main importance of this study is to develop an easily realizable synthesis to obtain practically applicable observer based state feedback controller which provides best performance while taking the unmeasurable states into account. At the end of the study, effectiveness of the proposed controller is illustrated through simulations under bump and random runway excitation. Simulation results indicate that the proposed observer based optimal controller having pole location constraint is all effective in improving the comfort of the passenger-crew and provides better road holding performance to enhance the braking and maneuvering performance during taxiing. In addition, actuator dynamics and actuator saturation phenomenon will be considered for the further study on the control of active landing gears.

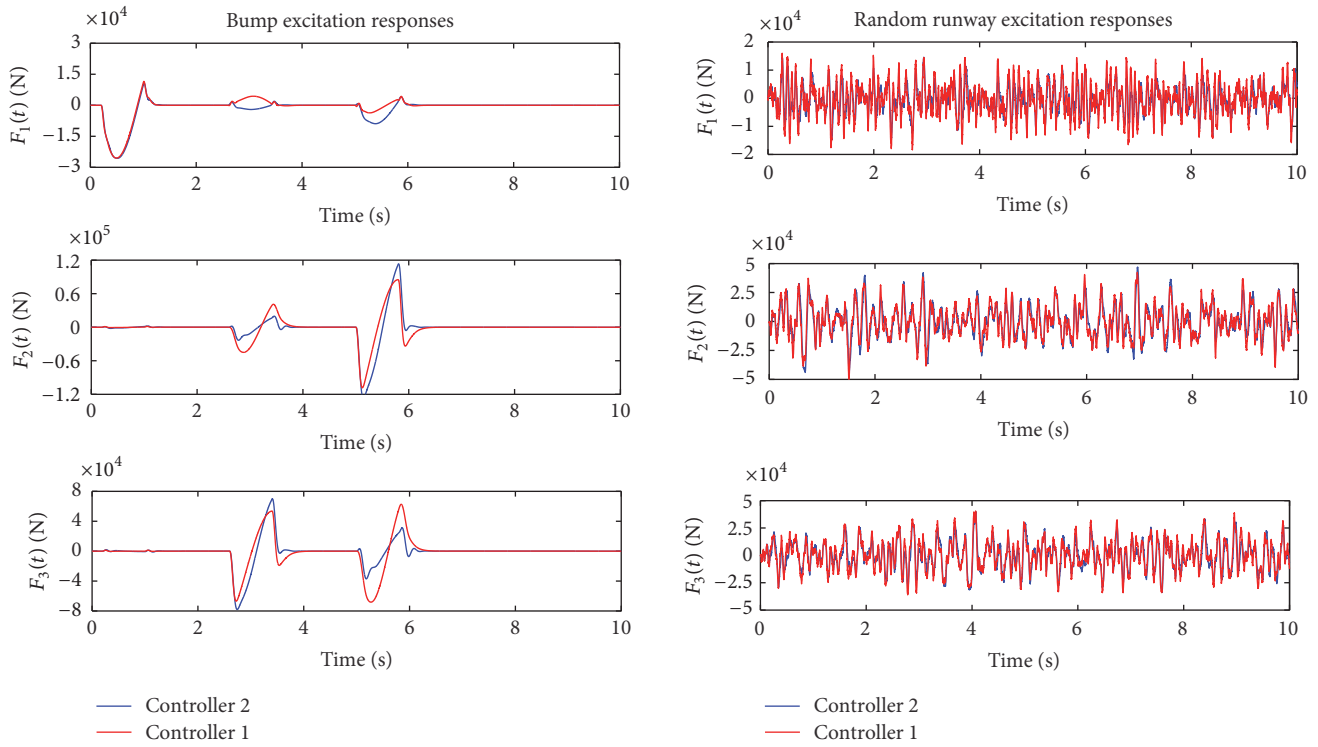

Figure 9: Time history of the applied control forces.

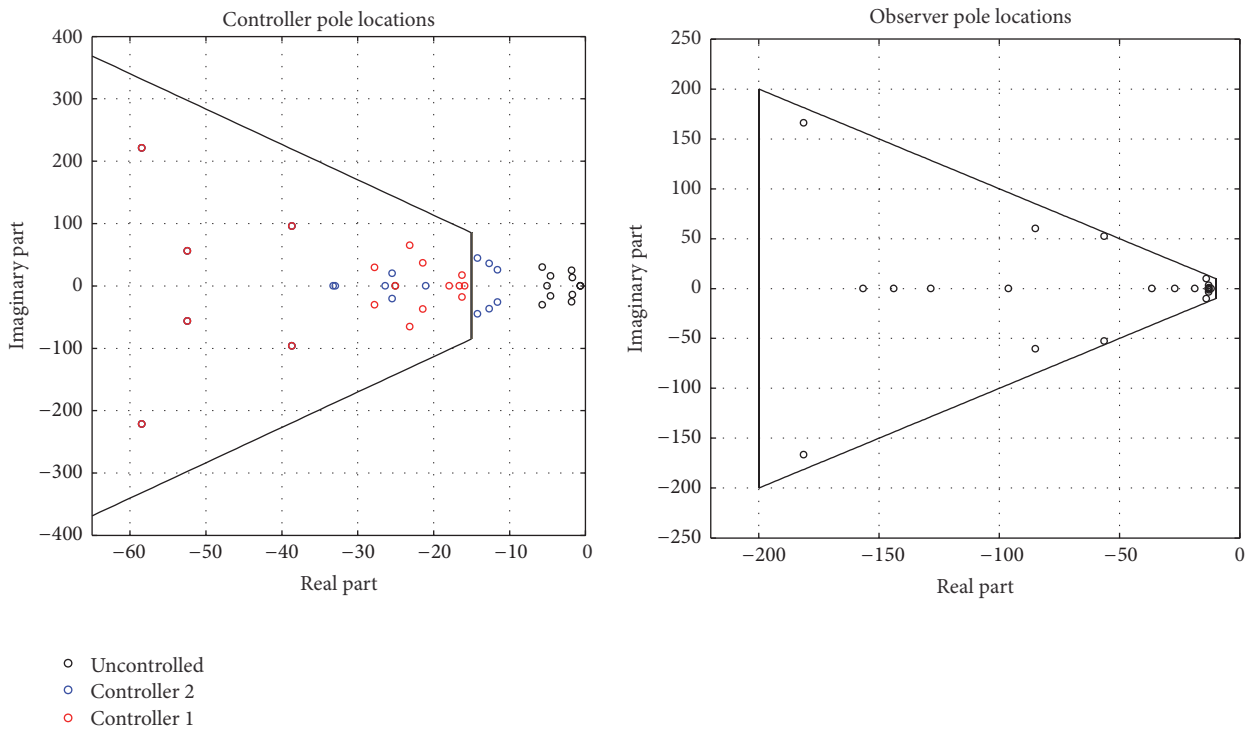

Figure 10: Closed loop and observer pole locations.

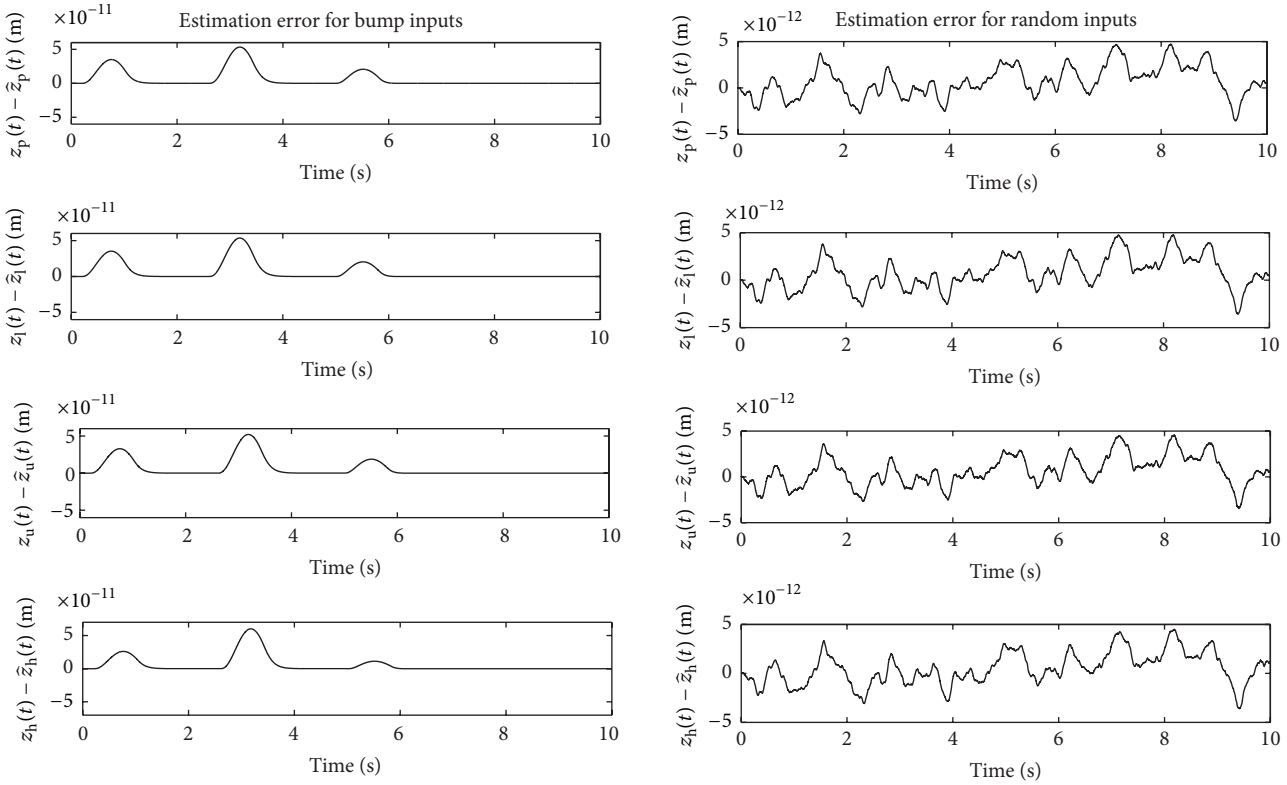

Figure 11: Observation performance.

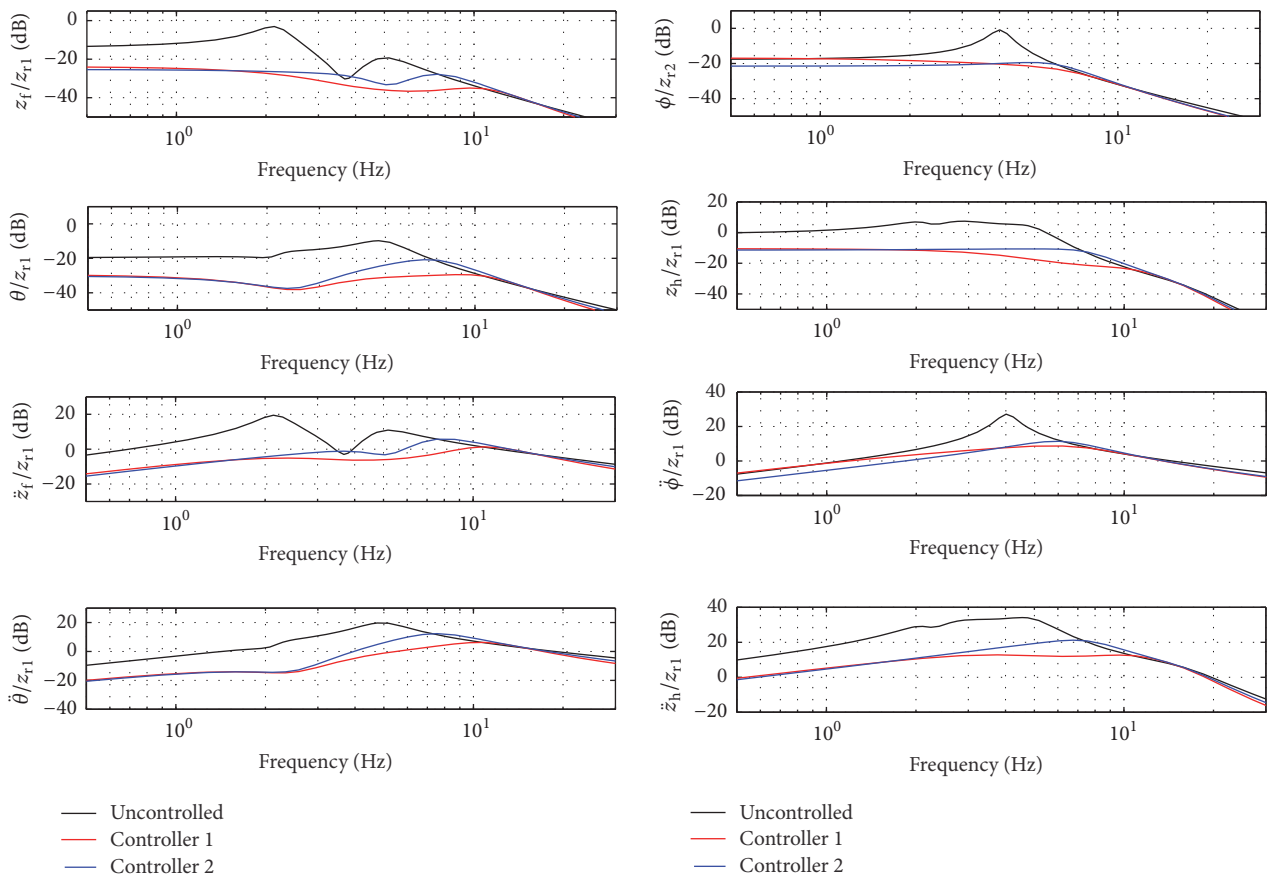

Figure 12: Controlled and uncontrolled frequency responses.

Appendix

Mass, damping, stiffness, disturbance input, and control input matrices are

$$M_s = \operatorname{diag}\left(m_1, m_s, m_3, I_x, I_y, m_f, m_s, m_p, m_l, m_u, m_h\right);$$

$$C_s = \begin{bmatrix} C_{s11} & C_{s12} \\ C_{s12}^T & C_{s22} \end{bmatrix},$$

$$K_s = \begin{bmatrix} K_{s11} & K_{s12} \\ K_{s12}^T & K_{s22} \end{bmatrix},$$

$$E_s = \begin{bmatrix} -\operatorname{diag}\left(k_{t1}, k_{t2}, k_{t3}\right) & -\operatorname{diag}\left(c_{t1}, c_{t2}, c_{t3}\right) \\ 0_{8\times3} & 0_{8\times3} \end{bmatrix},$$

$$F_s = \begin{bmatrix} F_{s1} \\ F_{s2} \\ F_{s3} \end{bmatrix},$$

$$C_{s11} = \begin{bmatrix} c_{t1}+c_{s1} & 0 & 0 & 0 & c_{s1}\ell_f \\ 0 & c_{t2}+c_{s2} & 0 & -c_{s2}\ell_{sl} & -c_{s2}\ell_r \\ 0 & 0 & c_{t3}+c_{s3} & c_{s3}\ell_{sr} & -c_{s3}\ell_r \\ 0 & -c_{s2}\ell_{sl} & c_{s3}\ell_{sr} & c_{s2}\ell_{sl}^2 + c_{s3}\ell_{sr}^2 + c_{fs}\ell_{ss}^2 & c_{s2}\ell_{sl}\ell_r - c_{s3}\ell_{sr}\ell_r \\ c_{s1}\ell_f & -c_{s2}\ell_r & -c_{s3}\ell_r & c_{s2}\ell_r\ell_{sl} - c_{s3}\ell_r\ell_{sr} & c_{s1}\ell_f^2 + c_{s2}\ell_r^2 + c_{s3}\ell_r^2 + c_{fs}\ell_{sf}^2 \end{bmatrix},$$

$$C_{s12} = \begin{bmatrix} -c_{s1} & 0 & 0 & 0 & 0 & 0 \\ -c_{s2} & 0 & 0 & 0 & 0 & 0 \\ -c_{s3} & 0 & 0 & 0 & 0 & 0 \\ c_{s2}\ell_{sl} - c_{s3}\ell_{sr} + c_{fs}\ell_{ss} & -c_{fs}\ell_{ss} & 0 & 0 & 0 & 0 \\ -c_{s1}\ell_f + c_{s2}\ell_r + c_{s3}\ell_r - c_{fs}\ell_{sf} & c_{fs}\ell_{sf} & 0 & 0 & 0 & 0 \end{bmatrix},$$

$$C_{s22} = \begin{bmatrix} c_{s1}+c_{s2}+c_{s3}+c_{fs} & -c_{fs} & 0 & 0 & 0 & 0 \\ -c_{fs} & c_{fs}+c_{sp} & -c_{sp} & 0 & 0 & 0 \\ 0 & -c_{sp} & c_{sp}+c_{pl}+c_{pu} & -c_{pl} & -c_{pu} & 0 \\ 0 & 0 & -c_{pl} & c_{pl}+c_{lu} & -c_{lu} & 0 \\ 0 & 0 & -c_{pu} & -c_{lu} & c_{pu}+c_{lu}+c_{uh} & -c_{uh} \\ 0 & 0 & 0 & 0 & -c_{uh} & c_{uh} \end{bmatrix},$$

$$K_{s11} = \begin{bmatrix} k_{t1}+k_{s1} & 0 & 0 & 0 & k_{s1}\ell_f \\ 0 & k_{t2}+k_{s2} & 0 & -k_{s2}\ell_{sl} & -k_{s2}\ell_r \\ 0 & 0 & k_{t3}+k_{s3} & k_{s3}\ell_{sr} & -k_{s3}\ell_r \\ 0 & -k_{s2}\ell_{sl} & k_{s3}\ell_{sr} & k_{s2}\ell_{sl}^2 + k_{s3}\ell_{sr}^2 + k_{fs}\ell_{ss}^2 & k_{s2}\ell_{sl}\ell_r - k_{s3}\ell_{sr}\ell_r \\ k_{s1}\ell_f & -k_{s2}\ell_r & -k_{s3}\ell_r & k_{s2}\ell_r\ell_{sl} - k_{s3}\ell_r\ell_{sr} & k_{s1}\ell_f^2 + k_{s2}\ell_r^2 + k_{s3}\ell_r^2 + k_{fs}\ell_{sf}^2 \end{bmatrix},$$

$$K_{s12} = \begin{bmatrix} -k_{s1} & 0 & 0 & 0 & 0 & 0 \\ -k_{s2} & 0 & 0 & 0 & 0 & 0 \\ -k_{s3} & 0 & 0 & 0 & 0 & 0 \\ k_{s2}\ell_{sl} - k_{s3}\ell_{sr} + k_{fs}\ell_{ss} & -k_{fs}\ell_{ss} & 0 & 0 & 0 & 0 \\ -k_{s1}\ell_f + k_{s2}\ell_r + k_{s3}\ell_r - k_{fs}\ell_{sf} & k_{fs}\ell_{sf} & 0 & 0 & 0 & 0 \end{bmatrix},$$

$$K_{s22} = \begin{bmatrix} k_{s1}+k_{s2}+k_{s3}+k_{fs} & -k_{fs} & 0 & 0 & 0 & 0 \\ -k_{fs} & k_{fs}+k_{sp} & -k_{sp} & 0 & 0 & 0 \\ 0 & -k_{sp} & k_{sp}+k_{pl}+k_{pu} & -k_{pl} & -k_{pu} & 0 \\ 0 & 0 & -k_{pl} & k_{pl}+k_{lu} & -k_{lu} & 0 \\ 0 & 0 & -k_{pu} & -k_{lu} & k_{pu}+k_{lu}+k_{uh} & -k_{uh} \\ 0 & 0 & 0 & 0 & -k_{uh} & k_{uh} \end{bmatrix},$$

$$F_{s1} = -I_{3\times 3},$$

$$F_{s2} = \begin{bmatrix} 0 & \ell_{sl} & -\ell_{sr} \\ -\ell_f & \ell_r & \ell_r \\ 1 & 1 & 1 \end{bmatrix},$$

$$F_{s3} = 0_{5\times 3}. \tag{A.1}$$

Competing Interests

The authors declare that they have no competing interests.

References

[1] J. R. McGebee and H. D. Carden, "Matmematical model of an active control landing gear for load control during impact and roll-out," NASA Technical Note D-8080, Langley Research Center, Hampton, Va, USA, 1976.

[2] D. Howe, *Aircraft Loading and Structural Layout*, Professional Engineering Publishing, London, UK, 2004.

[3] N. S. Currey, *Aircraft Landing Gear Design: Principles and Practice*, AIAA Education Series, 1998.

[4] R. Freymann, "Actively damped landing gear system," in *Proceedings of the Landing Gear Design Loads Conference*, No. 20, AGARD CP-484, 1991.

[5] W. E. Howell, J. R. Mc Gehee, R. H. Daugherty, and W. A. Vogler, "F-106B airplane active control landing gear drop test performance," in *Proceedings of the Landing Gear Design Loads Conference*, no. 21, AGARD CP-484, Long Beach, Calif, USA, October 1991.

[6] C.-C. Liang and C.-F. Chiang, "A study on biodynamic models of seated human subjects exposed to vertical vibration," *International Journal of Industrial Ergonomics*, vol. 36, no. 10, pp. 869–890, 2006.

[7] T. Catt, D. Cowling, and A. Shepherd, "Active landing gear control for improved ride quality during ground roll," SDL Report 232, Stirling Dynamics Limited, Bristol, UK, 1992.

[8] F. A. C. Viana, V. Steffen Jr., M. A. X. Zanini, and L. Goes, "Identification of a non-linear landing gear model using nature-inspired optimization," *Shock and Vibration*, vol. 15, no. 3-4, pp. 257–272, 2008.

[9] G. Mikułowski and Ł. Jankowski, "Adaptive landing gear: optimum control strategy and potential for improvement," *Shock and Vibration*, vol. 16, no. 2, pp. 175–194, 2009.

[10] I. P. Jocelyn, "An overview of landing gear dynamics," NASA TM-209143, 1999.

[11] B. W. Payne, A. E. Dudman, B. R. Morris, and M. Hockenbull, "Aircraft dynamic response an repaired runways," AGARD CP-326, 1982.

[12] M. Zapateiro, F. Pozo, J. Rossel, H. R. Karimi, and N. Luo, "Landing gear suspension control through adaptive backstepping techniques with H Performance," in *Proceedings of the 18th IFAC World Congress*, vol. 2, pp. 4809–4814, Milano, Italy, September 2011.

[13] Y. H. Jia, "Taxiing performance analysis of active control of landing gear," *Acta-Aeronautica et Astronoutica, Snica*, vol. 20, no. 6, pp. 545–548, 1999.

[14] W. Krüger, "Design and simulation of semi-active landing gears for transport aircraft," *Mechanics of Structures and Machines*, vol. 30, no. 4, pp. 493–526, 2002.

[15] H. Wang, J. T. Xing, W. G. Price, and W. Li, "An investigation of an active landing gear system to reduce aircraft vibrations caused by landing impacts and runway excitations," *Journal of Sound and Vibration*, vol. 317, no. 1-2, pp. 50–66, 2008.

[16] X. Wang and U. Carl, "Fuzzy control of aircraft semi-active landing system," in *Proceedings of the 37th AIAA Aerospace Sciences Meeting and Exhibit*, Reno, Nev, USA, 1999.

[17] L. G. Ghiringhelli and S. Gualdi, "Evaluation of a landing gear semi-active control system for complete aircraft landing," *Aerotechnica Missili e Spazio*, vol. 83, pp. 21–31, 2004.

[18] A. A. Gharapurkar, A. F. Jahromi, R. B. Bhat, and W.-F. Xie, "Semi-Active control of aircraft landing gear system using H_∞ control approach," in *Proceedings of the 2nd IEEE International Conference on Connected Vehicles and Expo (ICCVE '13)*, pp. 679–686, December 2013.

[19] B. Sateesh and D. K. Maiti, "Vibration control of an aircraft nose landing gear due to ground-induced excitation," *Proceedings of the Institution of Mechanical Engineers, Part G:*, vol. 224, no. 3, pp. 245–258, 2010.

[20] I. Ross and R. Edson, "Application of active controllanding gear technology to the A-10 aircraft," NASA CR-166104, Langley Research Center, Hampton, Va, USA, 1983.

[21] R. Freymann, "An experimental-analytical routine for the dynamic qualification of aircraft operating on rough runway surfaces," AGARD Report 731, 1987.

[22] S. Sivakumar and A. P. Haran, "Mathematical model and vibration analysis of aircraft with active landing gears," *Journal of Vibration and Control*, vol. 21, no. 2, pp. 229–245, 2015.

[23] W. Abbas, O. B. Abouelatta, M. El-Azab, M. Elsaidy, and A. A. Megahed, "Optimization of biodynamic seated human models using genetic algorithms," *Engineering*, vol. 2, no. 9, pp. 710–719, 2010.

[24] S. Boyd, L. El Ghaoui, E. Feron, and V. Balakrishnan, *Linear Matrix Inequalities in System and Control Theory*, vol. 15 of *SIAM Studies in Applied Mathematics*, Society for Industrial and Applied Mathematics, Philadelphia, Pa, USA, 1994.

[25] H. Yazici, R. Guclu, I. B. Kucukdemiral, and M. N. A. Parlakci, "Robust delay-dependent H_∞ control for uncertain structural systems with actuator delay," *Transactions of ASME, Journal of Dynamic Systems, Measurement and Control*, vol. 134, no. 3, pp. 1–15, 2012.

[26] H. Yazici, C. O. Azeloglu, and I. B. Kucukdemiral, "Active vibration control of container cranes against earthquake by the use of delay-dependent H_∞ controller under consideration of actuator saturation," *Journal of Low Frequency Noise, Vibration and Active Control*, vol. 33, no. 3, pp. 289–316, 2014.

[27] H. Du, W. Li, and N. Zhang, "Integrated seat and suspension control for a quarter car with driver model," *IEEE Transactions on Vehicular Technology*, vol. 61, no. 9, pp. 3893–3908, 2012.

[28] G. E. Dullerud and F. Paganini, *A Course in Robust Control Theory: A Convex Approach*, Springer, 2005.

[29] G.-R. Duan and H.-H. Yu, *LMIs in Control Systems: Analysis, Design and Applications*, CRC Press, 2013.

[30] M. Chilali and P. Gahinet, "H_∞ design with pole placement constraints: an LMI approach," *IEEE Transactions on Automatic Control*, vol. 41, no. 3, pp. 358–367, 1996.

[31] D. Arzelier, J. Bernussou, and G. Garcia, "Pole assignment of linear uncertain systems in a sector via a Lyapunov-type approach," *IEEE Transaction on Automatic Control*, vol. 38, no. 7, pp. 1128–1132, 1993.

[32] Y. Zhao, W. Sun, and H. Gao, "Robust control synthesis for seat suspension systems with actuator saturation and time-varying input delay," *Journal of Sound and Vibration*, vol. 329, no. 21, pp. 4335–4353, 2010.

[33] A. Giua, M. Melas, C. Seatzu, and A. G. Usai, "Design of a predictive semiactive suspension system," *Vehicle System Dynamics*, vol. 41, no. 4, pp. 277–300, 2004.

[34] S. Sivakumar and A. P. Haran, "Aircraft random vibration analysis using active landing gears," *Journal of Low Frequency Noise, Vibration and Active Control*, vol. 34, no. 3, pp. 307–322, 2015.

[35] J. Löfberg, "Yalmip: a toolbox for modelling and optimization in Matlab," in *Proceedings of the CACSD Conference*, pp. 284–289, Taipei, Taiwan, September 2004.

[36] J. F. Sturm, "Using SeDuMi 1.02, a Matlab toolbox for optimization over symmetric cones," *Optimization Methods and Software*, vol. 11, no. 1–4, pp. 625–653, 1999.

[37] F. Lin, *Robust Control Design: an Optimal Control Approach*, John Wiley & Sons, Berlin, Germany, 2007.

[38] ISO, "Mechanical vibration and shock evaluation of human exposure to whole body vibration," ISO 2631, International Standardization Organization, 1997.

[39] W. Sun, H. Gao, and O. Kaynak, "Finite frequency H_∞ control for vehicle active suspension systems," *IEEE Transactions on Control Systems Technology*, vol. 19, no. 2, pp. 416–422, 2011.